

ANALYSIS OF PISTON RING COATING USING PIN ON DISC SETUP

A THESIS SUBMITTED IN PARTIAL FULFILLMENT OF THE
REQUIREMENT FOR THE AWARD OF THE DEGREE OF

**MASTER OF TECHNOLOGY
(COMPUTATIONAL DESIGN)**

TO

DELHI TECHNOLOGICAL UNIVERSITY



SUBMITTED BY

AKSHAY SINGH

ROLL NO.- 2K14/CDN/20

UNDER THE GUIDANCE OF

DR. R. S. WALIA

ASSOCIATE PROFESSOR

DELHI TECHNOLOGICAL UNIVERSITY

**DEPARTMENT OF MECHANICAL, PRODUCTION & INDUSTRIAL
AND AUTOMOBILE ENGINEERING**

DELHI TECHNOLOGICAL UNIVERSITY

BAWANA ROAD, DELHI-110042

JUNE 2016



DELHI TECHNOLOGICAL UNIVERSITY

(Formerly Delhi College of Engineering)

Shahbad Daultapur, Bawana Road,

Delhi-110042

STUDENT'S DECLARATION

I, **Akshay Singh**, hereby certify that the work which is being presented in this thesis entitled “**Analysis of Piston Ring Coating using Pin on Disc Setup**” is submitted in the partial fulfillment of the requirement for degree of **Master of Technology (Computational Design)** in Department of Mechanical Engineering at **Delhi Technological University** is an authentic record of my own work carried out under the supervision of **Assoc. Prof. R. S. Walia**. The matter presented in this thesis has not been submitted in any other University/Institute for the award of Master of Technology Degree. Also, it has not been directly copied from any source without giving its proper reference.

Signature of Student

This is to certify that the above statement made by the candidate is correct to the best of my knowledge.

Signature of Supervisor



DELHI TECHNOLOGICAL UNIVERSITY

(Formerly Delhi College of Engineering)

Shahbad Daulatpur, Bawana Road,

Delhi-110042

CERTIFICATE

This is to certify that this thesis report entitled, “**Analysis of Piston Ring Coating Using Pin on Disc Setup**” being submitted by **Akshay Singh (Roll No. 2K14/CDN/20)** at Delhi Technological University, Delhi for the award of the Degree of Master of Technology as per academic curriculum. It is a record of bonafide research work carried out by the student under my supervision and guidance, towards partial fulfillment of the requirement for the award of Master of Technology degree in Computational Design. The work is original as it has not been submitted earlier in part or full for any purpose before.

Mr. S. M. Pandey

Assistant Professor

Mechanical Engineering

Delhi Technological University

Delhi-110042

Dr. R. S. Walia

Associate Professor

Mechanical Engineering Department

Delhi Technological University

Delhi-110042

ACKNOWLEDGEMENT

First and foremost, praises and thanks to the God, the Almighty, for His showers of blessings throughout my research work to complete the research successfully.

I would like to extend my gratitude to **Prof. R. S. Mishra, Head**, Department of Mechanical Engineering, Delhi Technological University, for providing this opportunity to carry out the present thesis work.

The constant guidance and encouragement received from **Mr. S. M. Pandey, Assistant Professor**, Department of Mechanical Engineering, Delhi Technological University, has been of great help in carrying out the present work and is acknowledged with reverential thanks.

I would like to express my deep and sincere gratitude to my research supervisor, **Assoc. Prof. Dr. R. S. Walia**, Department of Mechanical Engineering, Delhi Technological University, for giving me the opportunity to do research and providing invaluable guidance throughout this research. His dynamism, vision, sincerity and motivation have deeply inspired me. He has taught me the methodology to carry out the research and to present the research works as clearly as possible. It was a great privilege and honor to work and study under his guidance. I would also like to thank him for his friendship, empathy, and great sense of humor. Without the wise advice and able guidance, it would have been impossible to complete the thesis in this manner.

I would like to express my special gratitude and thanks also to my juniors **Deependra Shukla & Sahib Kalra** in developing the project, who have willingly helped me out with their abilities. I wish them all the very best for their future endeavors. I am also grateful to all the faculty members of the Mechanical Engineering Department for molding me at correct time so that I can have a touch at final destination and to all my friends, for the help, moral support and encouragement; they had given to me during completion of dissertation work.

I am extremely grateful to my parents and family for their love, prayers, caring and sacrifices for educating and preparing me for my future.

AKSHAY SINGH
M.Tech. (COMPUTATIONAL DESIGN)
2K14/CDN/20

ABSTRACT

The performance of computers and the development of software products enabled the implementation of capable simulation tools also for tribological applications. The system behaviour of friction and wear makes it necessary to combine different tools and to consider different scales in modelling. Using the data and parameters of experiments done in research papers, we correlate the operating parameters of obtain desirable result. And prepare a model of dry sliding wear between pin on disc in Abaqus.

Tribological simulation can be seen as a new study problem developed from modern information technology and computer simulation technology in combination with a variety of mathematical methods in the field of tribology. Due to the complexity of actual tribological systems and different working conditions, the results obtained from traditional simulation test method were often qualitative only, and couldn't be used in designing of tribological systems and practical engineering applications. There is a need to seek new ways and means of in-depth study of the wear quantitative law, otherwise the fundamental breakthrough of the prevention and control of the wear could not be achieved. The tribological simulation research of the typical pin on disc sliding wear test system was carried by the adoption of computer technology and mathematical analysis methods in order to provide a new wear analysis method for the simulation of the basic tribological contact problems.

In this research work, the wear simulation model including multiple parameters was established based on experimental and theoretical data. The parameters of the model were determined by the test data. The simulation model reflects the basic relationship between input and output of the pin on disc dry sliding wear test. Simulation results shows that as the load on pin increase depth wear also increase with angular velocity remains the same and it also reveals the effect of pin diameter on wear depth.

Table of Contents

<u>Contents</u>	<u>Page No.</u>
STUDENT'S DECLARATION	i
CERTIFICATE	ii
ACKNOWLEDGEMENT	iii
ABSTRACT	iv
TABLE OF CONTENTS	v
LIST OF FIGURES	vii
LIST OF TABLES	ix
CHAPTER 1: INTRODUCTION	1-14
1.1 Tribology	1
1.2 Importance of Tribology	1
1.3 Piston Ring	2
1.3.1 Four major functions of Piston Ring	2
1.3.2 Piston Ring Type	3
1.3.3 Force analysis of Piston Ring	4
1.3.4 Failure of piston ring	4
1.4 Motivation	5
1.5 Introduction to Wear	6
1.6 Wear Measures	7
1.7 Types of Wear	8
1.8 Technique of friction force measurement	9
1.8.1 Strain gauged beams	9
1.8.2 Simultaneous measurement of load and friction force	10
1.8.3 Determination of wear by profilometry	10
1.9 Thermal spray coating	11
1.9.1 Types of Thermal Spray coating	12
CHAPTER 2: LITERATURE REVIEW	15-24
2.1 Literature of FEM	15
2.2 Literature of coating	19
CHAPTER 3: MATHEMATICAL MODEL	25-32
3.1 Numerical Analysis	25
3.2 Nonlinear solution methods in Abaqus/Standard	25
3.3 Finite Element Formulations of Contact Problems	30
3.4 The Penalty Method	30
3.5 Wear model (Archard's law)	32

CHAPTER 4: EXPERIMENTAL PROCEDURE	33-44
4.1 Sample preparation	33
4.2 Coating preparation	33
4.2.1 Plasma arc spray coating	34
4.2.2 Moly Powder Description	36
4.2.3 Some remarkable point about the Plasma Spray Coating Machine	37
4.3 Design of Experiment	38
4.4 Pin on disc test	39
4.5 Scanning electron microscope	40
4.6 X -Ray diffractometer	42
4.7 Vickers micro hardness tester	43
CHAPTER 5: ANALYSIS BY SIMULATION SOFTWARE	45-53
5.1 Part Module	45
5.2 Property Module	46
5.3 Assembly Module	48
5.4 Step Module	49
5.5 Interaction Module	49
5.6 Load module	50
5.7 Mesh module	51
5.8 Job Module	52
5.9 Visualization	52
CHAPTER 6: RESULTS AND DISCUSSION	53-63
CHAPTER 7: CONCLUSION AND FUTURE SCOPE	64
7.1 Conclusion	64
7.2 Future scope	64
References	65-67

Table of Figures

Chapter 1	Introduction	
Fig. 1.1	Piston Ring with terminology	3
Fig. 1.2	Force diagram of piston ring	4
Fig. 1.3	Friction transducer applying a combination of strain gauges on a flexible beam	10
Fig. 1.4	Schematic diagram of thermal spray coating	12
Fig. 1.5	Schematic diagram of wire flame spray	12
Fig. 1.6	Schematic diagram of power flame spray	13
Fig. 1.7	Schematic diagram of plasma spray	13
Fig. 1.8	Schematic diagram of electric arc wire spray	14
Fig. 1.9	Schematic diagram of high velocity oxy-fuel spray	14
Chapter 3	Mathematical model	
Fig. 3.1	Contact element-penalty method formulation	31
Chapter 4	Experimental Procedure	
Fig. 4.1	Schematic diagram of air plasma arc spray	33
Fig. 4.2	Coating formation on the sample by air plasma arc spray machine	35
Fig. 4.3	Plasma Spray Coating machine unit	35
Fig. 4.8	Tribometer setup in DTU, Delhi	39
Fig. 4.9	Clamped coated plate and pin in tribometer	39
Fig. 4.10	Scanning electron microscope in DTU, Delhi	41
Fig. 4.11	X-Ray diffractometer in DTU, Delhi	43
Fig. 4.12	Micro hardness indentation	44
Chapter 5	Analysis by Simulation Software	
Fig. 5.1	3D Model of pin	45
Fig. 5.2	3D model of disc	46
Fig. 5.3	Assembly of pin on disc	48
Fig. 5.4	Loading Condition	51
Fig. 5.5	Meshed Assembly View	52
Chapter 6	Results and Discussion	
Fig. 6.1	Contact Pressure at 70N loading condition	54

Fig. 6.2	Contact Pressure at 60N loading condition	55
Fig. 6.3	Contact Pressure at 50N loading condition	55
Fig. 6.4	Contact pressures at the contact interface of pin and disc	56
Fig. 6.5	Temperature by ABAQUS and experiment at 70N loading	57
Fig. 6.6	Temperature by ABAQUS and experiment at 60N loading	57
Fig. 6.7	Temperature by ABAQUS and experiment at 50N loading	58
Fig. 6.8	Temperature at the contact interface of pin and disc	59
Fig. 6.9	Heat flux vector distribution at 70N loading condition	59
Fig. 6.10	Heat flux vector distribution at 60N loading condition	60
Fig. 6.11	Heat flux vector distribution at 50N loading condition	60
Fig.6.12	Heat Flux Vector at the contact interface of pin and disc	61
Fig. 6.13	Frictional coefficient of coating material between pin and disc	62
Fig. 6.14	Specific wear rate vs load	62

List of Tables

Chapter 1 Introduction

Table 1.1	Various types of wear, their symptoms & appearance	8
-----------	--	---

Chapter 4 Experimental Procedure

Table 4.1	Air Plasma arc coating's operation conditions	34
Table 4.2	SEM Image of sample powders	36
Table 4.3	Composition of the final mixture ready for coating	37
Table 4.4	Important control parameter of air plasma spray coating	37
Table 4.5	Boundary Conditions for the test	38
Table 4.6	Variables for wear test	38

Chapter 5 Analysis by Simulation Software

Table 5.1	Composition of coating material	46
Table 5.2	Properties of materials	47
Table 5.3	properties of pin and disc materials	48
Table 5.4	Interaction properties for load 50 N	49
Table 5.5	Interaction Properties for load 60N	50
Table 5.6	Interaction Properties for load 70N	50
Table 5.7	Boundary conditions for three different loading conditions	50

Chapter 6 Results and Discussions

Table 6.1	Angular velocities of disc	54
Table 6.2	Contact pressures according to load	56
Table 6.3	Contact pressures according to load	58
Table 6.4	Specific wear rate and coefficient of friction with respect to load	63

CHAPTER 1

INTRODUCTION

1.1 Tribology

The term tribology is derived from the Greek tribos, which means rubbing and includes all of the sciences and technologies of interacting surfaces in relative motion. The main areas of research and application are friction, wear, and lubrication. The term was first used 1966 in the Jost Report, a study conducted in the United Kingdom which investigated the amount of money lost annually due to friction and wear [1]. Tribology is multidisciplinary in nature, and includes mechanical engineering (especially machine elements as journal and roller bearings and gears), materials science, with research into wear resistance, surface technology with surface topography analysis and coatings, and the chemistry of lubricants and additives. The relatively younger disciplines of tribology are: (i) bio-tribology, which includes (among other topics) wear, friction, and the lubrication of total joint replacement; and (ii) nanotribology, where friction and wear are studied on the micro- and nanoscales.

1.2 Importance of Tribology

Over the years, the governments of the most industrialized countries have developed extensive strategies to reduce energy waste. In 1966, the so-called Jost Report demonstrated the enormous waste that occurred due to the misrecognition of tribology in the UK. Likewise, in 1977, an American government-financed report suggested that US\$16.25 billion could be saved by the correct use of tribological knowledge. Similar studies have also been conducted in other countries; for example, W. Bartz carried out a study which related to Germany between 1979 and 1983 [1] while in 1990 P. Jost defined the potential savings as a percentage of the GDP, to determine calculated values of 1.3–1.6%. The results obtained for various countries are listed in Table 1.1, taking 1.6% as a basis for the year 2008 (a conservative estimate when taking actual energy prices into account). In this case, the GDP was based on the CIA, List of Fact Book (2008). Notably, whilst the study of W. Bartz takes into account only lubricated contacts, it categorizes the possibilities of saving into: (i) primary savings, due to reductions in mechanical friction; (ii) secondary savings, due to a lesser exchange of machine parts owing to wear reduction; and (iii) tertiary savings, where a new material is used for the production of new parts, thus raising the energy content of the

materials [1]. Currently, the integration of tribology represents a modern aspect in life cycle assessment, with the main targets being environmental and economic performance. In this case, the main roles of tribology are not only to reduce friction in a machine, but also to extend the machines service life.

1.3 Piston Ring

Piston ring is located between the cylinder and the piston, piston rings are necessary components that allow the engine to operate efficiency. It fits into the groove of the outer diameter of piston in internal combustion engine.

1.3.1 Four major functions of Piston Ring

- 1. Compression gas sealing** -Piston rings maintain gas compression between the piston and the cylinder wall.

Piston rings seal the cylinder so that combustion gas generated at the time of ignition does not leak into the opening between the piston and the cylinder. If combustion gas leaks, the engine cannot output sufficient power, increasing fuel consumption. Not good both in terms of economy and the environment.

- 2. Lubrication oil film control-** Piston rings usually make necessary minimum lubricating oil film for preventing scuffing.

Since gas ignition is repeated many times, the piston goes up and down inside the engine at a rate of several thousand times per minute. A small amount of oil is poured over the pistons so they move smoothly, with little friction between metal and metal. Piston rings adjust the amount of oil.

- 3. Heat transfer-** Piston rings transfer heat from the piston crown to the cylinder.

When gas ignition takes place, the temperature inside a piston reaches approximately 300 C. If heat accumulates inside the piston, the engine may be damaged. For that reason, it is necessary to release the heat build-up. Piston rings help release this heat.

- 4. Support piston in cylinder-** Piston rings prevent the piston from knocking on the cylinder wall.

If the piston inclines inside the cylinder, it may touch inside parts and cause engine failure as well. Piston rings support pistons to allow for smooth up and down motion.

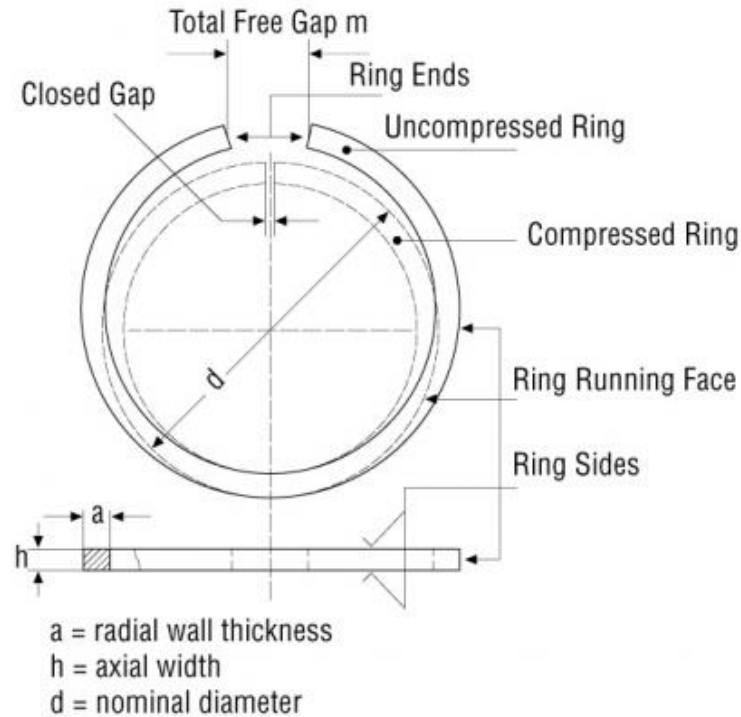


Fig. 1.1: Piston Ring with terminology [2]

1.3.2 Piston Ring Type

1. **Top Ring-** This is referred to as the upper compression ring. This ring operates under the harshest conditions with respect to thermal and mechanical loading. Its job is to form a gas-tight barrier between the piston and cylinder wall in order to seal the combustion chamber. They also transfer the heat to the cooled cylinder walls like a bridge.
2. **Second Ring-** This is referred to as the lower compression ring. One of its job is to work together with the top ring in order to seal the combustion chamber and transfer the heat to the cylinder walls. They also control oil consumption.
3. **Oil Control Ring-** Oil Control Rings regulate and limit oil consumption. They scrape off excess lubricating oil from the cylinder walls and return it to the

crankcase. They are designed to provide a thin oil film to ensure piston and ring lubrication.

1.3.3 Force analysis of Piston Ring

When the combustion takes place inside the chamber, a gas pressure force is exerted on two sides of piston ring (one is on top surface and other is on the right surface). Due to the motion of piston ring with a friction force is exerted on the sliding surface of ring. And inertia force is exerted on the piston ring.

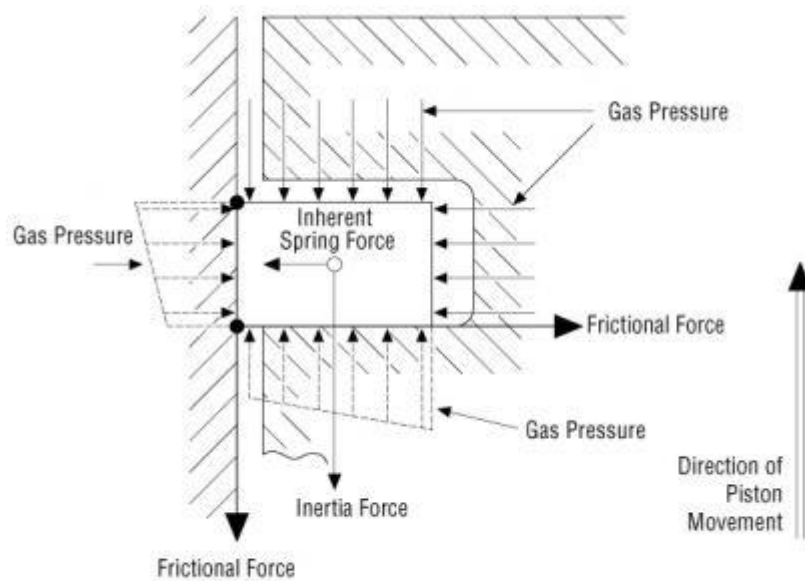


Fig. 1.2: Force diagram of piston ring [2]

1.3.4 Failure of piston ring

- **Top groove wear and top ring breakage**-The top groove shows the most wear since it is exposed to the highest temperatures and pressures and also it has the greatest exposure to airborne abrasives that may come in through the intake system. As wear occurs, the clearance between the ring and groove increases and the rate of wear accelerates. Following is a list of conditions that may cause top groove failure:
 - Airborne abrasives
 - Excessive deposits
 - Combustion knock Installation of a new ring in a worn groove

- Assembly of new rings without removing the wear ridge at the top of the cylinder.
- **Scuffing and Scoring-** Scuffing is invariably the result of excessive heat. It occurs when the surface temperature of one or both of two rubbing metal surfaces reaches the melting point of the material, allowing a small dab of the melted material to pull out. This leaves a void on one surface and a deposit cold-welded to the other surface. Scoring may be considered simply as a severe case of scuffing where the voids and scratches are much more apparent.

Scuffing may be identified by discoloured metal. When magnified, the metal will be burnished and smeared in the direction of motion.

1.4 Motivation

Due to the failure of piston ring, an engine's life is reduced. So the wear resistant material coating is one of the methods to increase life of engine. Coating material must with stand on high temperature, friction and pressure conditions.

1.5 Introduction to Wear

There are several precise definitions for wear. However, for engineering purposes the following definitions contains the essential elements [3].

- Wear is damage to a surface as a result of relative motion with respect to another substance. One key point is that wear is damage and it is not limited to loss of material from the surface. However, loss of material is definitely one way in which apart can experience wear.
- Another way included in this definition is by movement of material without loss of mass. An example of this would be the change of geometry or dimension of a part as a result of plastic deformation (e.g., from repeated hammering).
- There is also a third mode implied, which is damage to a surface that does not result in mass loss or dimensional changes. An example of this third mode might be development of network of cracks in a surface. This might be of significance in applications where maintaining optical transparency is a prime engineering concern.

Lens and aircraft windows are examples where this is an appropriate definition of wear.

In the older definitions of wear there used to be a greater stress on the “loss of material”, however now-a-days the newer and more general definitions of wear is very natural to the design or device engineer, who thinks of wear in terms of a change to a part that effects its performance. The focus is on the change which may be translated to damage. The implication of this generalization will be further explored in the discussion of wear measures.

1.6 Wear Measures

Previously wear was defined as damaged to a surface. The most common form of that damage is loss or displacement of material and volume can be used as a measure of wear-volume of material removed or volume of material displaced. For scientific purposes this is frequently the measure used to quantify wear. In many studies, particularly material investigations, mass loss is frequently the measure used instead of volume. This is done because of the relative ease of performing a weight loss measurement. However, there are some problems in using mass as primary measure of wear.

- Direct comparison of materials can only be done if their densities are same. For bulk material this is not a major obstacle, since the density is either known or easily determined. In the case of coatings however, this can be a major problem. The other problems are more intrinsic ones.
- A mass measurement does not measure displaced materials. In addition, it is sensitive to wear debris and transferred material that becomes attached to the surface and cannot be removed. This material does not necessarily have to be from the same surface; it can from the counter face as well.







From the above it can be seen that volume is the fundamental measure for wear when wear is calculated with loss or displacement of material. However, in engineering applications, is generally with the loss of a dimension, the increase in clearance or change in contour not the volume loss.

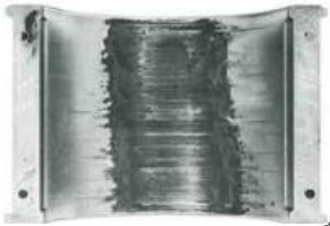
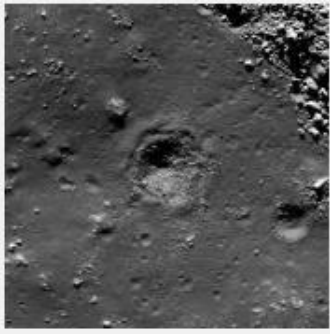
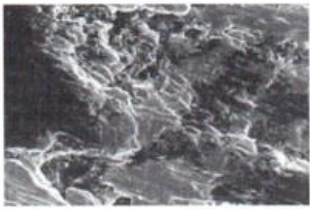
Volume, mass loss and a dimension are not the only measures for wear that are used in engineering. Life, vibration level, roughness, appearance, friction level, and degree of surface crack or crazing are some of the operational measures that are encountered.

1.7 Types of Wear

The various types of wear, their symptoms and appearance of the worn out surfaces are given below in Table 1.1.

Table 1.1 Various types of wear, their symptoms & appearance [2]

Types of wear	Symptoms	Appearance of the worn out surface	Diagram of wear
Abrasive	Presence of clean furrows cut out by abrasive particles	Seizure, catering rough and torn out surfaces Erosion	
Erosion	Presence of abrasives in the fast moving fluid and short abrasion furrows	Waves and troughs	
Corrosion	Presence of metal corrosion Products	Rough pits or depressions	
Impacts	Surface fatigue, small submicron particles or formation of spalls	Fragmentation, peeling and Pitting	
Fatigue	Presence of surface and sub surface cracks accompanied by pits and spalls	Sharp and angular edges around pits	
Delamination	Presence of surface cracks parallel to the surface with semi dislodged or loose flakes	Loose, long and thin sheet like particles	

Fretting	Production of voluminous amount of loose debris	Roughening, seizure and development of oxide ridges	
Electric attack	Presence of micro craters or a track with evidence of smooth molten metal	Smooth holes	
Adhesive	Metal transfer is a prime symptom	Seizure, catering rough and torn out surfaces	

1.8 Technique of friction force measurement

1.8.1 Strain gauged beams

Strain gauged beams are considerably cheaper and can be designed to suit almost any level of friction force. Friction force is usually measured from the bending of a beam arranged perpendicularly to the direction of the friction force. Measurement of friction force using the principle of a flexible beam is shown in Fig. 1.3. Frictional force, acting tangentially to a disc sample, is measured by recording changes in circuit resistance. From the friction force and the normal force (load) a coefficient of friction is calculated.

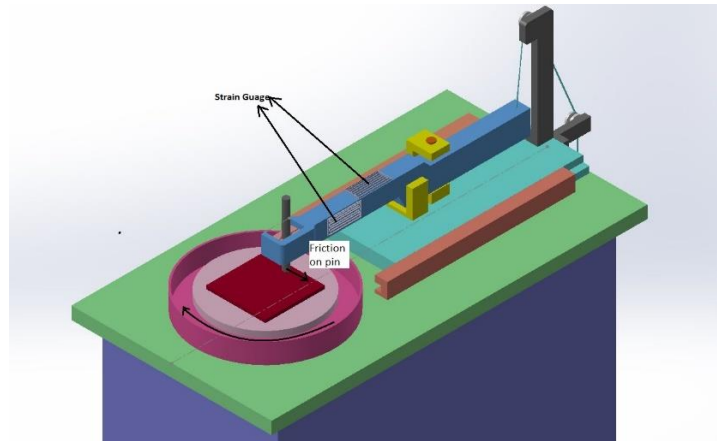


Fig. 1.3: Friction transducer applying a combination of strain gauges on a flexible beam

1.8.2 Simultaneous measurement of load and friction force

The instantaneous contact force should be continuously measured for exact determinations of the friction coefficient. This contact force can be measured by fitting strain gauge flexure elements that deflect with variations of force in the load axis. The flexure elements for friction force measurements. Simultaneous load and friction force measurement by the use of two strain gauged beams is shown in the Fig. 1.3.

1.8.3 Determination of wear by profilometry

A commonly used technique to evaluate the worn volume from the wear scar is profilometry. For this purpose, an optical projector, e.g. profile projector, stylus profilometry, e.g. talysurf, or laser scanning profilometry, eg. UBM are being used. These techniques are provided the information of topography of the wear scar and distribution of wear between specimens.

Optical projector can offer a simple yet sensitive technique of measuring wear changes in specimens that have a simple shape such as in pin. The technique is based on projecting an image of the object, e.g. pin, on a screen and measuring the change in dimensions of the silhouette of the worn specimen, [2]. One of the limitations of this technique is that distortion of pin by creep and attachment to the true worn profile.

The stylus profilometry technique provides a picture of the wear scar which is compiled by making several evenly spaced traverses of the stylus or laser over the wear scar. Wear can be assessed from the deepest wear scar profile thus detected or else the volume of the wear scar can be calculated by numerical integration of measured wear scar sections. The technique is, however, time consuming and is usually applied to record total wear at the end of a test.

In the scanning profilometry light from a semiconductor laser is focused on the surface measured generating a surface incident spot of approximately 1 [μm] in diameter. The spot is then imaged onto a sensor with photodiodes via the beam splitter. Combined output from the photodiodes gives the focus error signal. This signal is then used to control the position of the moveable objective lens within the sensor. The lens is moved in real time in such manner that the signal is always maximum, i.e. the focal spot of the beam always remains coincident with object surface. Surface displacement reproduced by the movement of the lens is then measured by the light balance system attached to the lens. The focus error signal can be added to the light falling on all diodes in the sensor resulting in 'reflecting intensity signal' which is used to generate microscope quantity images of the surface for general inspection over large lateral areas.

1.9 Thermal spray coating

Thermal spray is defined as applying these coatings takes place by means of special devices / systems through which melted or molten spray material is propelled at high speed onto a cleaned and prepared component surface. The coating feedstock material is melted by a heat source. This liquid or molten material is then propelled by process gases and sprayed onto a base material, where it solidifies and forms a solid layer. The individual aspect of a thermal sprayed coating follows.

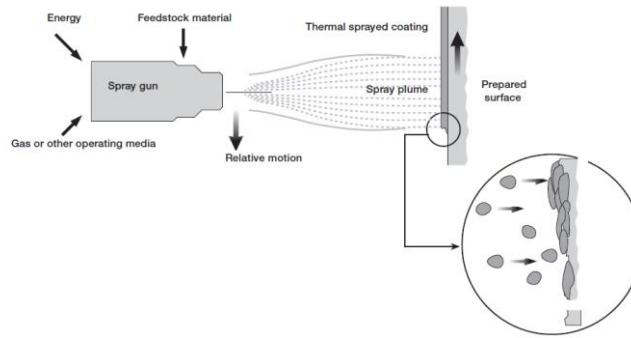


Fig. 1.4: Schematic diagram of thermal spray coating

1.9.1 Types of Thermal Spray coating

a) Wire Flame Spray- With the wire flame spray process, the wire spray material is melted in a gaseous oxygen-fuel flame. The fuel gas can be acetylene, propane or hydrogen. The wire is fed concentrically into the flame, where it is melted and atomized by the addition of compressed air that also directs the melted material towards the workpiece surface.

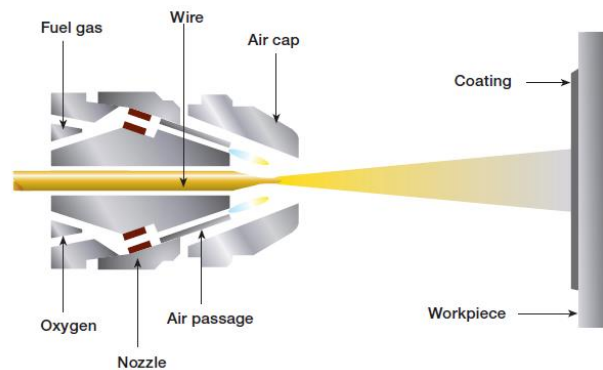


Fig. 1.5: Schematic diagram of wire flame spray

b) Powder Flame Spray- This coating process is based on the same operational principle as the wire flame spray process, with the difference that the coating material is a spray powder. Thus, a larger selection of spray materials is available, as not all spray materials can be manufactured in wire form. Electric Arc Wire Spray with electric arc wire spray, an arc is formed by contact of two oppositely charged metallic wires, usually of the same composition. This leads to melting at the tip of the wire material. Air atomizes the melted spray material and accelerates onto the substrate. The rate of spray is adjusted by appropriate regulation of the wire feed as it is melted, so a constant arc can be maintained.

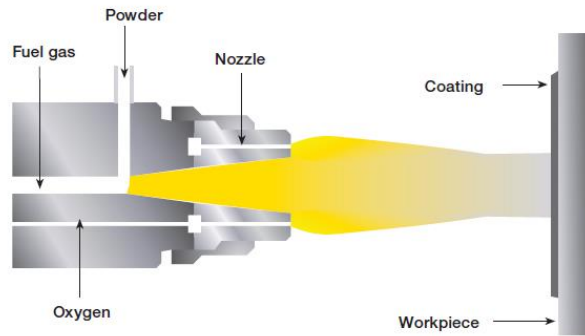


Fig. 1.6: Schematic diagram of power flame spray

c) **Plasma Spray**-The principle of plasma spraying is shown schematically in Fig. 1.7 a high frequency arc is ignited between an anode and a tungsten cathode. The gas flowing through between the electrodes (i.e., He, H₂, N₂ or mixtures) is ionized such that a plasma plumes several centimetres in length develops. The temperature within the plume can reach as high as 16000° K. The spray material is injected as a powder outside of the gun nozzle into the plasma plume, where it is melted, and hurled by the gas onto the substrate surface.

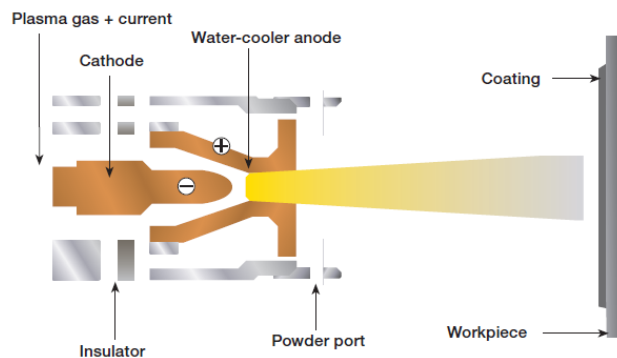


Fig. 1.7: Schematic diagram of plasma spray

d) **Electric Arc Wire Spray**- With electric arc wire spray, an arc is formed by contact of two oppositely charged metallic wires, usually of the same composition. This leads to melting at the tip of the wire material. Air atomizes the melted spray material and accelerates onto the substrate. The rate of spray is adjusted by appropriate regulation of the wire feed as it is melted, so a constant arc can be maintained.

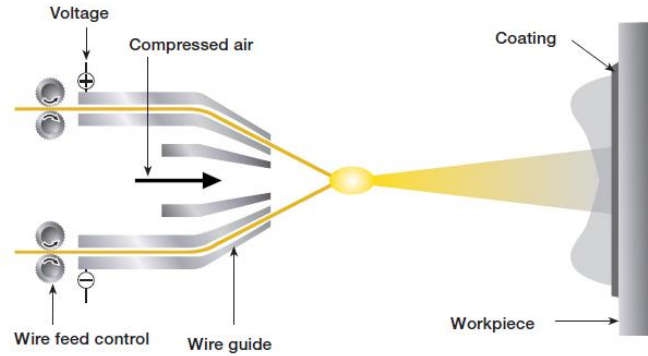


Fig. 1.8: Schematic diagram of electric arc wire spray

e) **The high velocity oxy-fuel spray (HVOF)-Process** is a relatively recent addition to the family of thermal spray processes. As it uses a supersonic jet, setting it apart from conventional flame spray, the speed of particle impact on the substrate is much higher, resulting in improved coating characteristics. The mechanism differs from flame spraying by an expansion of the jet at the exit of the gun (Fig. 1.9). Fuel gases of propane, propylene, acetylene, hydrogen and natural gas can be used, as well as liquid fuels such as kerosene.

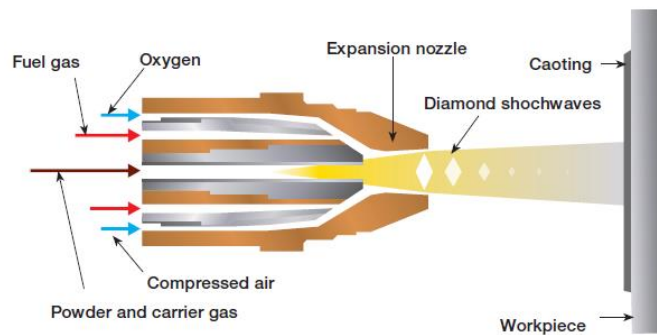


Fig. 1.9: Schematic diagram of high velocity oxy-fuel spray

CHAPTER 2

LITERATURE REVIEW

2.1 Literature of FEM

Bortoleto et al. [4] presented Experimental and numerical analysis of dry contact in the pin on disc test this work presents a computational study based on the linear Archard's wear law and finite element modelling (FEM), in order to analyse unlubricated sliding wear observed in typical pin on disc tests. Such modelling was developed using finite element software ABAQUSS with 3-Ddeformable geometries and elastic–plastic material behaviour for the contact surfaces. Archard's wear model was implemented into a FORTRAN user subroutine (UMESHMOTION) in order to describe sliding wear. Modelling of debris and oxide formation mechanisms was taken into account by the use of a global wear coefficient obtained from experimental measurements.

Kennedy et al [5] carried out a research on Contact temperatures and their influence on wear during pin-on-disk tribotesting presents some of the most useful analytical and numerical methods that can be used to predict surface temperature rises in dry or boundary lubricated pin-on-disk tribotests. The development of relatively simple, accurate, and easy-to-use expressions that can be used to predict contact temperatures in pin-on-disk sliding contacts. Wear of a ceramic (zirconia), metal (stainless steel) and polymer (polyethylene) in pin- on-disk tests are carried out.

Xinmin et al. [6] uses of pin-on-disc, they studied of the tribology characteristics of sintered versus standard steel gear materials and they simulate the sliding part of gear tooth contact in boundary and mixed lubricated regions, comparing the tribological characteristics of two sintered gear materials with those of a standard gear material. The comparison considered damage mechanisms, wear, and friction between these materials in different configurations (i.e., standard versus standard, sintered versus sintered, and sintered versus standard). The results indicate that, for pairings of the same gear materials, i.e., RS–RS (16MnCr5), AQ–AQ (Distaloy AQp0.2% C), and Mo–Mo (Astaloy 85Mop0.2% C), RS has a lower friction coefficient. For PM and RS combinations, both PM pins have lower friction coefficients with RS disc material than do RS pins with PM disc materials. For the wear coefficient, at low and

high speeds, RS pins always display better wear resistance than do AQ or Mo pins because of their high hardness and compacted microstructure. For RS–PM combinations, Mo pins display higher wear resistance than do AQ pins because their larger and more numerous pores enable good lubrication. Pins in the Mo–RS combination displayed the highest wear resistance, mainly because the pores in Mo discs hold lubricant, lubricating the contact surface and preventing adhesive wear. For the RS pin in the Mo–RS combination and the AQ pin in RS–AQ, the damage mechanism is slight adhesive wear and scuffing. For pins in the PM–PM, RS–PM, AQ–RS, and RS–RS combinations, the damage mechanism is a heavier scuffing-type adhesive wear.

Verma et al [7], Braking pad-disc system: Wear mechanisms and formation of wear fragments. The tribological phenomena that occur in brake systems are interesting even in other respects than just the braking action. One important issue, that is gaining increasing importance over the last years, concerns the environmental impact of wear debris produced by the braking action. In this context, the present study is focused on the tribological behavior of a commercial friction pad material dry sliding against a cast iron disc. Pin-on-disc tests were conducted at room temperature under mild wear conditions, as concerns load and rotating speed. The effect of some components of pad material, in particular of copper, on the dynamic of formation of tribological layer and wear debris is presented. The results obtained so, although referring to quite a simpler system than real brake systems, still may provide interesting indications, for instance in view of the development of novel brake pad materials and braking control systems.

Zmitrowicz [8] published a paper on ‘Wear patterns and laws of wear: a review’ and presented that wear is a process of gradual removal of a material from surfaces of solids subject to contact and sliding. Damages of contact surfaces are results of wear. They can have various patterns (abrasion, fatigue, ploughing, corrugation, erosion and cavitation). The results of abrasive wear are identified as irreversible changes in body contours and as evolutions of gaps between contacting solids. The wear depth profile of a surface is a useful measure of the removed material. The definition of the gap between contacting bodies takes into account deformations of bodies and evolutions of wear profiles. The wear depth can be estimated with the aid of wear laws. Derived in this study, constitutive equations of anisotropic wear are extensions of the Archard’s law of wear. The equations describe

abrasion of materials with microstructures. The illustrative example demonstrates calculations of the abraded mass and temperatures in pinon-disc test rig.

Guicciardi et al. [9] performed ten pin-on-disk sliding wear tests for each experimental condition were carried out with a commercial tungsten carbide (WC) pin on silicon carbide (SiC) disks in order to determine the wear and friction data dispersion. The tests were repeated using two sliding speeds (v), 0.1 and 1.0 m/s, and two applied loads (P), 5 and 50 N. The wear data showed a dispersion in the range of 28–47 and 32–56%, for disk and pin, respectively. For the disk, the dispersion decreased when increasing both sliding speed and applied load; for the pin, no clear relationship was found. The friction values spread in the range of 5–15%, with a lower dispersion at high applied load, independent of the sliding speed. From a statistical point of view, it was found that, in all the experimental conditions adopted, about 20% of the wear and friction values can be considered outliers.

PriitPodra, Soren Andersson [10] performed simulating sliding wear with finite element method, wear of components is often a critical factor influencing the product service life. Wear prediction is therefore an important part of engineering. The wear simulation approach with commercial finite element (FE) software ANSYS is presented in this paper. A modelling and simulation procedure is proposed and used with the linear wear law and the Euler integration scheme. Good care, however, must be taken to assure model validity and numerical solution convergence. A spherical pin-on-disc unlubricated steel contact was analysed both experimentally and with FEM, and the Lim and Ashby wear map was used to identify the wear mechanism.

It was shown that the FEA wear simulation results of a given geometry and loading can be treated on the basis of wear coefficient²sliding distance change equivalence. The finite element software ANSYS is well suited for the solving of contact problems as well as the wear simulation. The actual scatter of the wear coefficient being within the limits of ± 40 –60% led to considerable deviation of wear simulation results. These results must therefore be evaluated on a relative scale to compare different design options.

P. Prabhu [11] Finite element analysis usually neglects the contributions of wear and the changes in the surface due to wear. However, wear may be important in any structure subjected to repeated loadings and may be critical for certain tribological applications including the prediction of the sealing potential of surfaces. In this paper, a procedure is

proposed whereby the effects of wear may be calculated and included in the overall analysis of the structure. The Archard's equation is used as the basis for calculating wear strain which is used to modify the elastic strain in an element in an explicit manner. Extensions of the theory are also proposed and an example using explicit creep for the wear adjustments is included.

Imam Syafa at al [12] performed experiment two surfaces are brought in contact, deformation takes place at asperity level. The local pressure distribution and deformation of the contacting surfaces are importance with respect to wear. This paper describes a wear model to predict the wear of rough sliding contacts. The wear model is based on the general Archard's wear equation in combination with finite element analysis (FEA). In this paper the roughness is represented by uniformly distributed spherical asperities. The proposed model, FE in combination with Archard's wear law, has proven to be a powerful tool in predicting wear of rough surfaces.

S. C. Lim [13] developed the wear map model, this paper presents a summary of the author's personal view of the development of wear-mechanism maps, culminating in the presentation of some recently proposed maps. These maps, which present wear data in a graphical manner, are able to provide a more global picture of how materials in relative motions behave when different sliding conditions are encountered; they also provide the relationships between various dominant mechanisms of wear that are observed to occur under different sliding conditions as well as the anticipated rates of wear. Some thoughts on future directions for research in this area are also presented.

2.2 Literature review of coating

Yang [14] performed pin-on-disc wear tests of tungsten carbide inserts against hot-work tool steel disc. The experimental parameters selected in this research work are: (i) applied loads of 40 and 50 kgf; (ii) speeds of 100 and 130 m/min; (iii) temperatures of 25, 200, 400 and 600 °C; (iv) distances from 1000 to 16,000 m. It should be noted that the load and speed selected are close to those values used previously in the turning experiment. This is to facilitate the comparison of the wear coefficient values obtained from the previous study with the current one.

Two types of insert (pin) settings were used. With the first type, the insert was set in full contact with the disc throughout the whole testing cycle. In the second type, the insert was set with an initial angle with the disc at the beginning of the wear test, but would have a full contact at the end of the testing cycle. Two types of wear volume loss against distance values were obtained in this investigation, VA and VF, for inserts with an initial angular setting with the counter disc and those with a full contact with the counter disc, respectively. This work has provided a significant new insight into the discrepancy of the wear coefficient values obtained previously by the turning method and those by the standard pin-on-disc testing method.

Yucong Wang et al. [15] in their research describes a quick and reproducible bench scuffing and wear test which has utilized real piston skirts and engine cylinder bore sections with conformed contacts to determine the tribological characteristics of the sliding contact between the piston skirt and the cylinder bore counter face. Saturn 1.9 l L-4 engine parts were used for the wear and scuffing simulation tests. Two reciprocating bench test machines were used in evaluating the tribological behavior of coated piston/bore materials. To simulate the motion of pistons against cylinder bores in engine operation, test specimens were cut from the pistons and cylinder liners so that the piston skirt conforms to the cylinder wall. In the wear and scuff bench tests, the cylinder bore specimen was stationary.

The following test conditions were used to simulate normal wear: duration- 20h; temperature- 125°C; stroke- 6.77 mm; frequency- 10 Hz; load- 120 N; test lubricant- SAE 5W-30 and quantity- 8 ml (for wear tests only). A data acquisition system kept track of the coefficient of friction, the contact potential (or electric contact resistance), and changes in test parameters, such as the temperature.

R. Novak and T. Polcar [16] analyze in detail the uncertainty of friction coefficient measured by the standard pin-on-disc apparatus and the corresponding coating wear rate. Then we report application of the method to two large set of substrates, one coated by titanium nitride (TiN), the second with hydrogenated diamond like carbon coating (DLC). We determine the most significant contributors to the overall measurement uncertainty, which could help to either re-design the experiment procedure to reduce the measurement uncertainty or to simplify it by neglecting some parameters. We show that estimation of uncertainties could help to distinguish between random value variation and true trends (i.e. dependence of measured values on selected variable or set of variables).

Sharma et al. [17] work was focused on pin on disc tribometer, which is an advanced tribometer with precise measuring of friction and wear properties of combination of metals and lubricants under selected conditions of load, speed and temperature. The model used runs at very low rpm, at constant sliding velocity and fixed radius of wear circle. Data acquisition includes maximum depth of penetration and specific wear rate for both aluminium and mild steel. The specific wear rate is calculated; the specific wear rate helps in determining wear resistance provided by the metal under running conditions. This research relates to the various aspects (coefficient of friction, wear patten, lubrication testing, result graphs) obtained by pin on disc tribometer.

E.M. Bortoleto et al. [18] analyzed the T1 wear regime transition considering the pin on disc system and two different steels in dry contact. Analysis was conducted by means of both numerical simulation (FEM) and experimental tests. Pin on disc tests were conducted without lubrication, following ASTM G99-05 standard, which describes the conditions for sample geometry and preparation.

The test was carried out for 3600 s, corresponding a distance of 360 m. The normal load applied varied from 5 to 140 N, with 5 repetitions for each load condition. The values of friction coefficient were determined by the ratio between friction load and applied normal load. The variation of mass was determined from measurements conducted on a scale with precision of $1e-5$ g.

To produce a general FEM model, able to predict wear in more complex geometries systems by using input parameters obtained from experimental wear tests. Furthermore, this is a first step to create the background needed to investigate in depth the friction and wear phenomena in real systems, e.g. piston ring-cylinder contact in internal combustion engines

Johanssona et al. [19] work was related to the development and verification of a methodology capable of mimicking the real engine behavior at boundary and mixed lubrication regimes in order to minimize frictional losses and wear. This work focused on the development of test rig methodology and to investigate present and future candidate materials.

By using real production components (as opposed to simplified geometries) that contain the correct surface morphology, coating thickness and material composition the best component comparison to the real engine tests is made.

It was however not possible in a simplified tribometer experiment to utilize the same speeds, loads and temperatures as can be found in the engine. The objective was thus to find a parameter that can compare the contact of the top piston ring against the cylinder liner in the engine and in the tribometer.

You Wang et al. [20] evaluated the abrasive wear resistance of the ceramic coatings using diamond abrasives. They used the plasma spray technique to deposit coatings with reconstituted nanostructured $\text{Al}_2\text{O}_3/\text{TiO}_2$ powders. The abrasive wear tests were performed on a modified grinding/polishing machine. Abrasion rates (wear rates) are calculated using the mean measurement value of three samples in terms of the volume of material removed per unit load and distance of sliding against the diamond abrasive pad.

Both as fabricated and after wear $\text{Al}_2\text{O}_3/\text{TiO}_2$ coatings were investigated by X-ray diffraction, SEM and indentation tests. The abrasive wear mechanism is also discussed.

Titanium carbide, like other transition metal carbides, has useful properties including a low friction coefficient, high surface hardness, high melting point (3067 °C) as well as thermal and chemical stability. **Alexander Sivkov et al. [21]** explained the possibility of TiC/Ti coating deposition on a copper substrate using a high speed plasma jet, generated by the coaxial magneto plasma accelerator (CMPA). The average hardness of the deposited coating was determined and found to be about 1900 HV. The value of the critical adhesion strength was estimated to be 5200 MPa. Such a strong adhesion can be explained by hydrodynamic mixing of the main elements in the liquid state, during crystallization process, and deep penetration of coating particles into the substrate.

A study by **Tom Peat et al. [22]** provides insight on the erosion-corrosion performance of HVOF deposited WC-CoCr, Cr_3C_2 -NiCr and Al_2O_3 based coatings under slurry liquid

impingement. Through the use of liquid impingement apparatus, results will provide an indication of the three coatings' performance under conditions reflecting a flowing environment. The mass loss as a result of erosion, corrosion and the synergy factor has been calculated for each coating in order to generate comparative data for the relative performance of each coating material under multiple angles of attack. Metallographic analysis was carried out to establish a link between coating properties and the mode of coating degradation through assessment of wear scar damage. This body of work seeks to provide a novel insight on the erosion corrosion performance of WC-CoCr, Cr₃C₂-NiCr and Al₂O₃ based coatings under slurry liquid impingement through comparative analysis of the three coatings under consistent flowing erosion-corrosion conditions.

Guo Yan Fu et al. [23] developed a new glass coating to prevent the oxidation of the 20MnSiNb structural steel. The glass coating used in this study mainly consisted of metasilicate, chromium oxides and sodium silicate binder.

They also evaluated the anti-oxidation ability by the weight changes of 20MnSiNb samples which were heated in a muffle furnace. The samples were heated from room temperature to different temperatures, such as 800 °C, 900 °C, 1000 °C, 1050 °C, 1100 °C and 1150 °C, and maintained for 60 min. Finally, the possible protection mechanism of the coating was also investigated.

C. Verdon et al. [24] studied the measurement of the wear resistance of WC-Co coatings deposited by the HVOF process, as a function of the deposition conditions.

The HVOF thermal spraying of the powders on the austenitic stainless steel substrate was performed by Sulzer-Metco AG. Two different coatings were produced from the same powder of nominal composition WC88-Co12%wt using two different sets of spraying parameters. The main difference between those was the fuel gas used, i.e. H₂ or C₃H₈ for coating 1 and 2, respectively.

The erosion damages were observed in SEM along coating surface and transverse section. Special attention is paid to correlating the wear resistance to the coating microstructure, the latter being closely related to the spraying conditions.

Xiaohong Shi et al. [25] prepared a novel kind of SiC and La-Mo-Si-O-C coating by pack cementation and SAPS, respectively to enhance the oxidation resistance of C/C composites. To alleviate the mismatch of thermal expansion coefficient between outer coating and C/C

composites, the SiC internal coating was first prepared by pack cementation for C/C composites. The oxidation test of coating was conducted under 1773 K with static air. The phase composition, microstructures and oxidation resistance property of the La-Mo-Si-O-C coating have been studied.

Cecilia Bartulia et al. [26] studied fabrication of plasma sprayed ZrB₂-SiC ceramic coatings and tested them for high temperature oxidation resistance. The particular attention was focused on ZrB₂-SiC ceramic composites. An alternative fabrication technology, based on plasma spraying, was investigated to produce near net shape components. Thick Coatings were produced by controlled atmosphere plasma spray (CAPS), over a wide range of processing pressures.

Thermogravimetric and high temperature X-ray diffraction analyses were carried out to investigate the mechanism of formation of a potentially protective layer on the surface of exposed samples.

Elizabeth Withey et al. [27] attempted to reduce the compatibility issues between Haynes 230 and the Cu-Mg-Si PCM using three plasma sprayed metal oxide coatings: ZrO₂-20 wt.%Y₂O₃, Y₂O₃, and Al₂O₃. To understand the capability of these coatings as effective barriers against PCM attack of Haynes 230, sub-sized containment vessels were used to simulate the conditions of a single cycle of the thermal energy storage system. The chosen coating materials are known to be stable oxides. Reaction of the oxide coatings with the PCM, along with penetration of the coatings by one or more elements of the PCM, was found to determine failure in the investigated coatings.

Yulei Zhang et al. [28] in their work selected the ZrB₂-SiC-ZrC ceramic as the ablation coating for C/C composites and supersonic atmosphere plasma spraying (SAPS) was employed to prepare this coating due to the high temperature of a plasma arc and the high velocity of particles. Between the C/C substrate and the UHTC coating, a SiC buffer layer was sprayed to alleviate the mismatch. The purpose of this work is to describe the microstructure evolution of the coating as a function of different ablation time. The ablation mechanism of C/C composites with the multilayer coating is also discussed.

M. Tului et al. [29] work aims at developing a thermal spraying process, alternative to the CVD. A powder suitable for thermal spraying was prepared by means of spray dryer

agglomeration. ZrB_2 powder was sprayed using a commercial plasma spray equipment called controlled atmosphere plasma spray (CAPS). The usefulness of the simplified model to optimize the spray parameters was verified. Then, a simplified model of the plasma spray process was applied to optimize the spray parameters. Finally, the tribological and electrical properties of sprayed coatings were tested.

Pengf-ei He et al. [30] presented an internal plasma spraying fabrication process for a TiO_2 -based ceramic coating reinforced by 12 wt% Al_2O_3 (referred to as “TAC”). The microstructure, mechanical properties and areal surface topographies of the coating were characterized. And the reciprocating tribometer experiments were carried out to simulate engine acceleration from cruise to full power. The corresponding friction parameters of load, frequency and temperature were varied from 53 to 157N, from 35 to 45Hz, and from 85 to 197.5 °C respectively. Then, the tribological results and the wear mechanisms were analyzed and compared with uncoated cylinder barrels as a reference material (referred to as “REF”). As the objects for all tests, Lycoming 6-cylinder air-cooled horizontally-opposed aircraft piston engine IO-540-K was used.

CHAPTER 3

MATHEMATICAL MODEL

3.1 Numerical Analysis

Numerical analysis is the study of algorithms that use numerical approximation for the problems of mathematical analysis. Such problems originate generally from real-world applications of algebra, geometry and calculus, and they involve variables which vary continuously; these problems occur throughout the natural sciences, social sciences, engineering, medicine, and business.

In our problem of the frictional contact analysis, we used ABAQUS to solve and solver of the software uses the solution technique as Full Newton technique which is Newton's method as a numerical technique for solving nonlinear equilibrium equations.

3.2 Nonlinear solution methods in Abaqus/Standard

The finite element models generated in Abaqus are usually nonlinear and can involve from a few to thousands of variables. In terms of these variables the equilibrium equations obtained by discretizing the virtual work equation can be written symbolically as

$$F^N(u^M) = 0, \quad (3-1)$$

Where F^N is the force component conjugate to the N^{th} variable in the problem and u^M is the value of the M^{th} variable. The basic problem is to solve equation 3.1 for the u^M throughout the history of interest.

Many of the problems to which Abaqus will be applied are history-dependent, so the solution must be developed by a series of “small” increments. Two issues arise: how the discrete equilibrium statement equation 3.1 is to be solved at each increment, and how the increment size is chosen.

Abaqus/Standard generally uses Newton's method as a numerical technique for solving the nonlinear equilibrium equations. The motivation for this choice is primarily the convergence rate obtained by using Newton's method compared to the convergence rates exhibited by alternate methods (usually modified Newton or quasi-Newton methods) for the types of

nonlinear problems most often studied with Abaqus. The basic formalism of Newton's method is as follows. Assume that, after an iteration i , an approximation u_i^M , to the solution has been obtained. Let c_{i+1}^M be the difference between this solution and the exact solution to the discrete equilibrium equation Equation 3.1. This means that

$$F^N(u_i^M + c_{i+1}^M) = 0, \quad (3-2)$$

Expanding the left-hand side of this equation in a Taylor series about the approximate solution u_i^M then gives

$$F^N(u_i^M) + \frac{\partial F^N}{\partial u^P}(u_i^M)c_{i+1}^P + \frac{\partial^2 F^N}{\partial u^P \partial u^Q}(u_i^M)c_{i+1}^P c_{i+1}^Q + \dots = 0, \quad (3-3)$$

If u_i^M is a close approximation to the solution, the magnitude of each c_{i+1}^M will be small, and so all but the first two terms above can be neglected giving a linear system of equations:

$$K_i^{NP} c_{i+1}^P = -F_i^N \quad (3-4)$$

Where

$$K_i^{NP} = \frac{\partial F^N}{\partial u^P}(u_i^M) \quad (3-5)$$

is the Jacobian matrix and

$$F_i^N = F^N(u_i^M) \quad (3-6)$$

The next approximation to the solution is then

$$u_{i+1}^M = u_i^M + c_{i+1}^M \quad (3-7)$$

and the iteration continues.

Convergence of Newton's method is best measured by ensuring that all entries in F_i^N and all entries in c_{i+1}^M are sufficiently small. Both these criteria are checked by default in an Abaqus/Standard solution. Abaqus/Standard also prints peak values in the force residuals, incremental displacements, and corrections to the incremental displacements at each iteration so that the user can check for these contingencies himself.

Newton's method is usually avoided in large finite element codes, apparently for two reasons. First, the complete Jacobian matrix is sometimes difficult to formulate; and for some problems it can be impossible to obtain this matrix in closed form, so it must be calculated numerically an expensive (and not always reliable) process. Secondly, the method is

expensive per iteration, because the Jacobian must be formed and solved at each iteration. The most commonly used alternative to Newton is the modified Newton method, in which the Jacobian in Equation is recalculated only occasionally (or not at all, as in the initial strain method of simple contained plasticity problems). This method is attractive for mildly nonlinear problems involving softening behavior (such as contained plasticity with monotonic straining) but is not suitable for severely nonlinear cases. (In some cases Abaqus/Standard uses an approximate Newton method if it is either not able to compute the exact Jacobian matrix or if an approximation would result in a quicker total solution time. For example, several of the models in Abaqus/Standard result in a non-symmetric Jacobian matrix, but the user is allowed to choose a symmetric approximation to the Jacobian on the grounds that the resulting modified Newton method converges quite well and that the extra cost of solving the full nonsymmetric system does not justify the savings in iteration achieved by the quadratic convergence of the full Newton method. In other cases the user is allowed to drop interfield coupling terms in coupled procedures for similar reasons.)

Another alternative is the quasi-Newton method, in which Equation is symbolically rewritten

$$c_{i+1}^P = -[K_i^{NP}]^{-1}F_i^N \quad (3-8)$$

and the inverse Jacobian is obtained by an iteration process.

There are a wide range of quasi-Newton methods. The more appropriate methods for structural applications appear to be reasonably well behaved in all but the most extremely nonlinear cases—the trade-off is that more iterations are required to converge, compared to Newton. While the savings in forming and solving the Jacobian might seem large, the savings might be offset by the additional arithmetic involved in the residual evaluations (that is, in calculating the F_i), and in the cascading vector transformations associated with the quasi-Newton iterations. Thus, for some practical cases quasi-Newton methods are more economic than full Newton, but in other cases they are more expensive. Abaqus/Standard offers the “BFGS” quasi-Newton method: it is described in “Quasi-Newton solution technique,”

When any iterative algorithm is applied to a history-dependent problem, the intermediate, non-converged solutions obtained during the iteration process are usually not on the actual solution path; thus, the integration of history-dependent variables must be performed completely over the increment at each iteration and not obtained as the sum of integrations

associated with each Newton iteration, c_i . In Abaqus/Standard this is done by assuming that the basic nodal variables, u , vary linearly over the increment, so that

$$u(\tau) = \left(1 - \frac{\tau}{\Delta t}\right)u(t) + \frac{\tau}{\Delta t}u(t + \Delta t) \quad (3-9)$$

where $0 \leq \tau \leq \Delta t$ represents “time” during the increment. Then, for any history-dependent variable, $g(t)$, we compute

$$g(t + \Delta t) = g(t) + \int_t^{t+\Delta t} \frac{dg}{d\tau}(\tau) d\tau \quad (3-10)$$

at each iteration.

The issue of choosing suitable time steps is a difficult problem to resolve. First of all, the considerations are quite different in static, dynamic, or diffusion cases. It is always necessary to model the response as a function of time to some acceptable level of accuracy. In the case of dynamic or diffusion problems time is a physical dimension for the problem and the time stepping scheme must provide suitable steps to allow accurate modelling in this dimension. Even if the problem is linear, this accuracy requirement imposes restrictions on the choice of time step. In contrast, most static problems have no imposed time scale, and the only criterion involved in time step choice is accuracy in modelling nonlinear effects. In dynamic and diffusion problems it is exceptional to encounter discontinuities in the time history, because inertia or viscous effects provide smoothing in the solution. (One of the exceptions is impact. The technique used in Abaqus/Standard for this is discussed in “Intermittent contact/impact,”) However, in static cases sharp discontinuities (such as bifurcations caused by buckling) are common. Softening systems, or unconstrained systems, require special consideration in static cases but are handled naturally in dynamic or diffusion cases. Thus, the considerations upon which time step choice is made are quite different for the three different problem classes.

Abaqus provides both “automatic” time step choice and direct user control for all classes of problems. Direct user control can be useful in cases where the problem behaviour is well understood (as might occur when the user is carrying out a series of parameter studies) or in cases where the automatic algorithms do not handle the problem well. However, the automatic schemes in Abaqus are based on extensive experience with a wide range of problems and, therefore, generally provide a reliable approach.

For static problems a number of schemes have been suggested for automatic step control [29]. Abaqus/Standard uses a scheme based predominantly on the maximum force residuals following each iteration. By comparing consecutive values of these quantities, Abaqus/Standard determines whether convergence is likely in a reasonable number of iterations. If convergence is deemed unlikely, Abaqus/Standard adjusts the load increment; if convergence is deemed likely, Abaqus/Standard continues with the iteration process. In this way excessive iteration is eliminated in cases where convergence is unlikely, and an increment that appears to be converging is not aborted because it needed a few more iterations. One other ingredient in this algorithm is that a minimum increment size is specified, which prevents excessive computation in cases where buckling, limit load, or some modeling error causes the solution to stall. This control is handled internally, with user override if needed. Several other controls are built into the algorithm; for example, it will cut back the increment size if an element inverts due to excessively large geometry changes. These detailed controls are based on empirical testing.

In dynamic analysis when implicit integration is used, the automatic time stepping is based on the concept of half-increment residuals [30]. The basic idea is that the time stepping operator defines the velocities and accelerations at the end of the step $t + \Delta t$ in terms of displacement at the end of the step and conditions at the beginning of the step. Equilibrium is then established at $t + \Delta t$ which ensures an equilibrium solution at the end of each time step and, thus, at the beginning and end of any individual time step. However, these equilibrium solutions do not guarantee equilibrium throughout the step. The time step control is based on measuring the equilibrium error (the force residuals) at some point during the time step, by using the integration operator, together with the solution obtained at $t + \Delta t$, to interpolate within the time step. The evaluation is performed at the half step $t + \Delta t/2$. If the maximum entry in this residual vector the maximum “half-increment residual” is greater than a user-specified tolerance, the time step is considered to be too big and is reduced by an appropriate factor. If the maximum half-increment residual is sufficiently below the user-specified tolerance, the time step can be increased by an appropriate factor for the next increment. Otherwise, the time step is deemed adequate. The algorithm is somewhat more complicated at traumatic events such as impact. Here, the time step can also be adjusted based on the magnitude of residuals in the first or second iteration following such events. Clearly, if these residuals are several orders of magnitude greater than those permitted, convergence is unlikely and the time step is altered immediately to avoid unproductive iteration. These

algorithms are discussed in more detail in “Intermittent contact/impact,” [31] as well as in the ABAQUS Analysis User's Guide. They are products of experience and many numerical experiments and have been shown to be effective in several problem areas of interest.

3.3 Finite Element Formulations of Contact Problems

There are two basic theories that, although different in their approaches, offer the desired solutions to body contact problems: the penalty function method and the Lagrange multipliers method. The main difference between them is the way they include in their formulation the potential energy of contacting surfaces. The penalty function method, due to its economy, has received a wider acceptance. The method is very useful when solving frictional contact problems, while the Lagrange method, based on multipliers, is known for its accuracy. The main drawback of the Lagrange method is that it may lead to ill converging solutions while the penalty formulation may lead to inaccurate ones. In the following the pure penalty, the augmented Lagrange methods will be presented.

3.4 The Penalty Method

The penalty method involves adding a penalty term to enhance the solving process. In contact problems the penalty term includes the stiffness matrix of the contact surface. The matrix results from the concept that one body imaginary penetrates the another (Wriggers et al., 1990).

The stiffness matrix of the contact surface is added to the stiffness matrix of the contacting body, so that the incremental equation of the Finite Element becomes

$$[K_b + K_c]u = F \quad (3-11)$$

Where: K_b is the stiffness matrix of contacting bodies; K_c – stiffness matrix of contact surface; u – displacement; F – force. The magnitude of the contact surface is unknown (Stein & Ramm, 2003), therefore its stiffness matrix, K_c , is a nonlinear term. The total load and displacement values are

$$F^{tot} = \sum \Delta F \quad (3-12)$$

$$u^{tot} = \sum \Delta u \quad (3-13)$$

Where: F_{tot} is the force vector; u_{tot} – displacement vector. To derive the stiffness matrix, the contact zone (encompassing the contact surface) is divided into a series of contact elements. The element represents the interaction between the surface nodes of one body with the respective element face of the other body. Fig. 3.1 shows a contact element in a two-dimensional application. It is composed of a slave node (point S) and a master line, connecting nodes 1 and 2. S_0 marks the slave node before the application of the load increment, and S marks the node after loading.

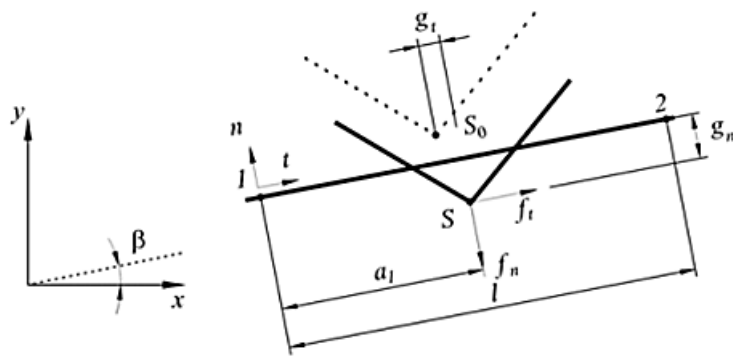


Fig. 3.1: Contact element-penalty method formulation

Given the nature of the numerical simulations presented afterwards only the sliding mode of friction will be presented. In this case, the tangential force acting at the contact surface equals the magnitude of the friction force, hence the first variation of the potential energy of a contact element is

$$\delta\pi_c = f_n \delta g_n + f_t \delta g_t = k_n g_n \delta g_t + \text{sgn}(g_t) \mu_d k_n g_n \delta g_t \quad (3-14)$$

Where: k_n represents penalty terms used to express the relationship between the contact force and the penetrations along the normal direction; k_t – penalty terms used to express the relationship between the contact force and the penetrations along the tangential direction; g_n – penetration along the normal direction; g_t – penetration along the tangential direction;

$$f_n = k_n g_n \quad (3-15)$$

$$f_t = -\text{sgn}(g_t) \mu_d (k_n g_n) \quad (3-16)$$

3.4 Wear model (Archard's law)

It is postulated by Archard that the total wear volume is proportional to the real contact area times the sliding distance. A coefficient K which is proportionality constant between real contact area, sliding distance and the wear volume has been introduced,

$$V = KA_r l = Kl \frac{W}{H} \quad (3-17)$$

Where

V is the wear volume [m³];

K is the proportionality constant;

A_r is the real area of the contact [m²];

W is the load [N];

H is the Vickers hardness of the softer surface [Pa];

l is the sliding distance [m];

The K coefficient is called as Archard coefficient, wear coefficient or wear constant. The low value of K indicates that wear is caused by only a very small proportion of small asperity contact.

The same term wear coefficient is defined by the following equation

$$k = \frac{V}{W * L} \quad (3-18)$$

Where

k is the specific wear rate (wear rate) [mm³/N-mm];

V is the wear volume [mm³];

W is the normal load [N];

L is the sliding distance [mm];

CHAPTER 4

EXPERIMENTAL PROCEDURE

4.1 Sample preparation

Casting means pouring molten metal into a mold with a cavity of the shape to be made, and allowing it to solidify. When solidified, the desired metal object is taken out from the mold either by breaking the mold or taking the mold apart. The solidified object is called the casting. Piston ring is always manufactured in circular shape for commercial use and it is very tough to manufacture a good quality piston ring with applied many finishing operations for desired shape. As per tribometer either we produce a pin of desired dimensions or we produce a disc of desired dimension. In this project we decided to develop a disc of a specific composition for the testing.

4.2 Coating preparation

Coating is the essential part of the completed product. Coating covers the surface of the product which is as the substrate. Coating is used to provide surface finish, corrosion resistance, wear resistance, appearance etc. In semiconductor device fabrication, coating is one of the important processes.

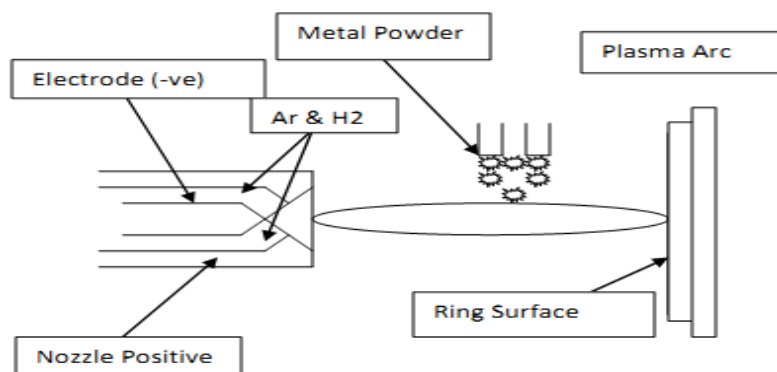


Fig. 4.1: Schematic diagram of air plasma arc spray

4.2.1 Plasma arc spray coating

One disc made of Piston Rings material (250X90X10 mm) was plasma sprayed with a Sulzer-Metco PT F4 torch in a closed room using a robot to ensure controlled and reproducible trajectories and speeds. The powder feeding system was a single bowl apparatus and the powder feed rate was fixed at 50 ± 5 gm/min. The discs were sand blasted with Al₂O₃ powder prior to spraying. During spraying, a cooling system consisting of air jets and Venturi nozzles was applied. In Table 4.1, the operating conditions are reported. A special attention was paid to the dependency of micro-structure and chemical composition of coatings on the nature of the plasma gas: Ar:H or Ar:He, the power off the plasma jet: 13–19.5 kW and the cooling device.

Table 4.1 Air Plasma arc coating's operation conditions

Sr. No	Process Parameter	Specification	Unit
1	Powder Port I.D.	2.2	mm
2	Water Flow Rate	4.0	Liter/min
3	Temperature of chiller	62	⁰ F
4	Distance between spray gun & mandrel	140(At gun angle 30 ⁰)	mm
5	Argon Flow Rate	112	m ³ /min
6	Hydrogen Flow Rate	13	m ³ /min
7	Argon Pressure	95	psi
8	Hydrogen Pressure	80	psi
9	Powder flow Rate	50	gm./min
10	Voltage	70	volt
11	Current	460	ampere
12	Gun Feed	10	mm./min
13	Gun Angle during spray	30	degree
14	Cooling air pressure	47	kgf
15	Powder driving temperature	120	⁰ C
16	Powder mixing	90	Min.



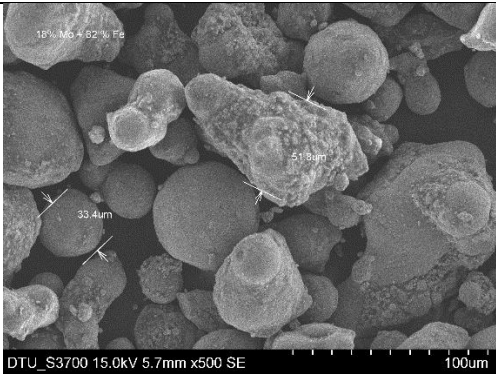

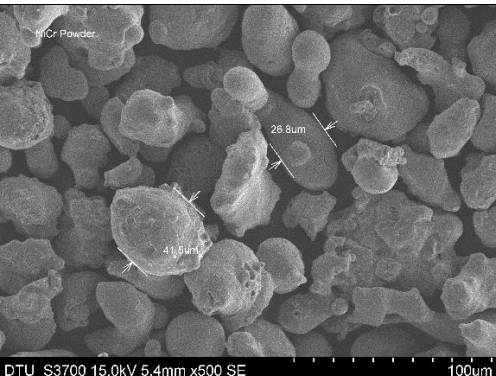
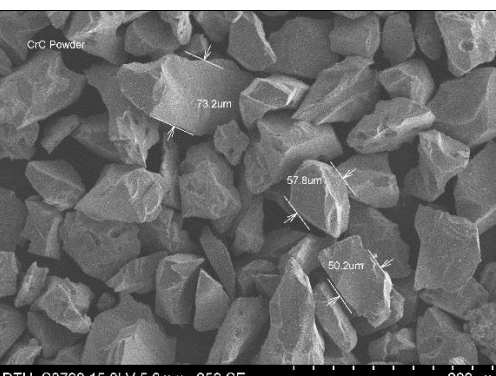
Fig. 4.2: Coating formation on the sample by air plasma arc spray machine



Fig. 4.3: Plasma Spray Coating machine unit

4.2.2 Moly Powder Description- Description of particle size and shape is shown in the following images. These images are taken from DTU Advanced Instrumentation Lab.

Table 4.2 SEM Image of sample powders

S. N.	Material	SEM Image
1	Fe+Mo	
2	Mo	
3	Ni-Cr	
4	CrC	

These all the Moly powder are mixed together with Binder & Slurry. Using this mixture, a lump of 50µm size is prepared. The mixture should be mixed properly to avoid the composition variation and to get the uniform property of coating after its preparation.

The approximate final composition of one charge is represented below in the table 4.5. The charge amount prepared for the coating is of 6 Kg.

Table 4.3 Composition of the final mixture ready for coating

Sr. No	Elements	Material Type	Quantity (Kg)
1	(63) Mo	Hard material	1.2
2	(43) NiCr	binder	0.6
3	(70) Cr ₃ C ₂	Hard material	0.6
4	(350) Fe Alloy	Base material	3.6

4.2.3 Some remarkable point about the Plasma Spray Coating Machine

Table 4.4 Important control parameter of air plasma spray coating

Sr. No	Parameter	Control
1	Bonding	8,000 – 9,000 PSI
2	Spray Rate	Can be increased by Increasing the Input Current
3	Choice of porosity	Porosity of deposit is higher
4	Choice of Coatings	Different metals, Combination of Metals, Ceramic can be deposited in desired quantity
5	Input	Metal in Powder form

In the Plasma Arc Spray Coating the Hydrogen is used as a secondary gas because 8000°C temperature produced by the Argon Gas (Argon temperature) is not enough to melt the high velocity powder particles. Thus to raise the temperature up to 10,000°C to 12,000°C for smoother melting of the mixture of powders we used Hydrogen (H₂).

4.3 Design of Experiment

To improve the quality of a product or process, Statistical methods are generally used. For the analysis of behavior of wear and friction of piston ring coating several factors (load and sliding speed) are considered in present work which tells the effect of every condition. To define the wear and frictional coefficient, one parameter (Load) required. There are number of methods to intend the experiment but we have selected constant sliding distance (2500m) and varying with sliding velocity of 1 m/s, 2 m/s, 3 m/s and with varying load of 50N, 60N, 70N (Table 4.8). To determine the response such as wear rate, microstructure, coefficient of friction, XRD analysis and EDS analysis.

Table 4.5 Boundary Conditions for the test

Variables	Level 1	Level 2	Level 3
Sliding speed (rpm)	319 rpm	764 rpm	1433 rpm
Load (N)	50N	60N	70N

Table 4.6 Variables for wear test

Coatings	Counter Body	Run	Load(N)	Sliding speed (rpm)	Track dia (mm)
Plasma Coating	Cylinder Liner	1	50	1m/s	60
Plasma Coating	Cylinder Liner	2	60	2 m/s	50
Plasma Coating	Cylinder Liner	3	70	3 m/s	40

4.4. Pin on disc test

Pin on disc type wear monitor with data acquisition system was used to evaluate the wear behavior of molybdenum alloys against pin of liner material. Load was applied on pin by dead weight through pulley string arrangement. The system had maximum loading capacity of 200 N. The test was performed under dry unlubricated condition. The wear test can be performed on any wear tester, but for thin coatings pin on disc wear test is most commonly used (figure 4.11).



Fig. 4.8: Tribometer setup in DTU, Delhi

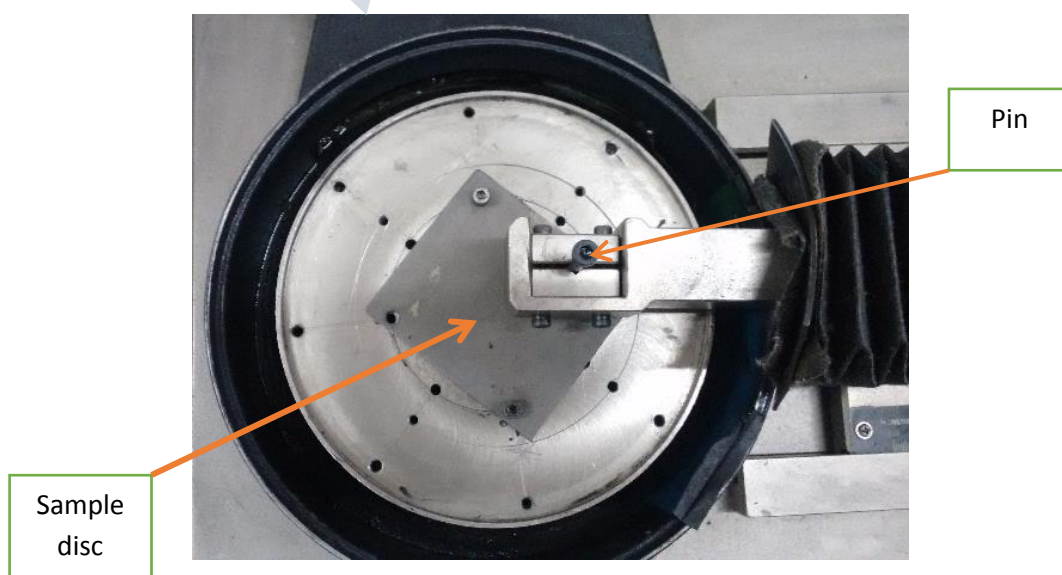


Fig. 4.9: Clamped coated disc and pin in tribometer

The machine is attached with the computer with software WINDCUM 2008. A window is open in the software and there are options to select various loads, times, pin diameter. The machine directly gives the coefficient of friction on the selected loading and sliding conditions. In this machine basically there is a rotating disc; and a pin is fixed over stainless steel pin holder. The pin can be loaded with different loads; it can be change externally. The coating pasted disc fastened on the machine with the help of screws. The load was applied on the pin through dead weight loading arrangement. The coating surface and pin was initially washed with methyl alcohol so that, moisture should not present on coating surface. Initially, the brass pin was fixed on the pin holder; the wear rate of the coatings was calculated at different loading and sliding conditions. The wear rate was calculated by weighing the disc before after the wear test in terms of grams on an electronic balance of least count 0.00001g. The load was taken as 50, 60 and 70 N respectively and the sliding speed was taken as 1 m/s, 2 m/s, 3 m/s & distance was taken 2500m. The wear behavior against three various counter pin material was analysed that was Nickel, En-31 and WC pin. The pin of diameter 10 mm was chosen for all of the three materials. The wear test carried out at room temperature of 24°C. During the wear test some amount of material also gets deposited on the pin in the form of a tribolayer so pin was cleaned after every test. So that there was always contact between pin and the coating surface, and the wear mechanism was between pin and coating surface, and a wear track was formed on the coating.

4.5 Scanning electron microscope

A scanning electron microscope (SEM) is a type of electron microscope that images a sample by scanning it with a high-energy beam of electrons in a raster scan pattern. The electrons interact with the atoms that make up the sample producing signals that contain information about the sample's surface topography, composition, and other properties such as electrical conductivity.



Fig. 4.10: Scanning electron microscope in DTU, Delhi

In a typical SEM, an electron beam is thermionically emitted from an electron gun fitted with a tungsten filament cathode. Tungsten is normally used in thermionic electron guns because it has the highest melting point and lowest vapour pressure of all metals, thereby allowing it to be heated for electron emission, and because of its low cost. For conventional imaging in the SEM, specimens must be electrically conductive, at least at the surface, and electrically grounded to prevent the accumulation of electrostatic charge at the surface. Metal objects require little special preparation for SEM except for cleaning and mounting on a specimen stub. Nonconductive specimens tend to charge when scanned by the electron beam, and especially in secondary electron imaging mode, this causes scanning faults and other image artifacts. They are therefore usually coated with an ultrathin coating of electrically-conducting material, commonly gold, deposited on the sample either by low vacuum sputter coating or by high vacuum evaporation. Conductive materials in current use for specimen coating include gold, gold/palladium alloy, platinum, osmium, iridium, tungsten, chromium and graphite. Coating prevents the accumulation of static electric on the

specimen during electron irradiation. For SEM, a specimen is normally required to be completely dry, since the specimen chamber is at high vacuum. Hard, dry materials such as wood, bone, feathers, dried insects or shells can be examined with little further treatment, but living cells and tissues and whole, soft-bodied organisms usually require chemical fixation to preserve and stabilize their structure. Fixation is usually performed by incubation in a solution of a buffered chemical fixative, such as glutaraldehyde, sometimes in combination with formaldehyde. In order to study the wear mechanism, the worn surface was examined by scanning electron microscope of S-3700 series in DTU, Delhi. To see the microstructure of the wear track the coating material is coated with gold. Then it was put on job holder, the job holder was then moved inside the chamber of the scanning electron microscope. The scanning electron microscopy was used to determine the surface morphology of the wear track which gave the wear mechanism at various loading conditions and various speeds. For SEM of samples following parameters were chosen that were Accelerating Voltage = 15000 Volt, Deceleration Voltage = 0 Volt, Magnification = 1000, Working Distance = 12600 μm , Emission Current = 80000 nA.

4.6. X-Ray diffractometer

X ray diffractometer is a measuring instrument for analyzing the structure of a material from the scattering pattern produced when a beam of radiation or particles (as X rays or neutrons) interacts with it. A typical diffractometer consists of a source of radiation, a monochromator to choose the wavelength, slits to adjust the shape of the beam, a sample and a detector. In a more complicated apparatus also a Gonio meter can be used for fine adjustment of the sample and the detector positions. When an area detector is used to monitor the diffracted radiation a beam stop is usually needed to stop the intense primary beam that has not been diffracted by the sample. Otherwise the detector might be damaged. Usually the beam stop can be completely impenetrable to the X-rays or it may be semitransparent. The use of semitransparent beam stop allows the possibility to determine how much the sample absorbs the radiation using the intensity observed through the beam stop. The specimen of the worn surfaces was placed on X-ray chamber. The scanning of the specimen was done from angle 20° to 90° and the scanning speed was chosen as 2 degree/min.

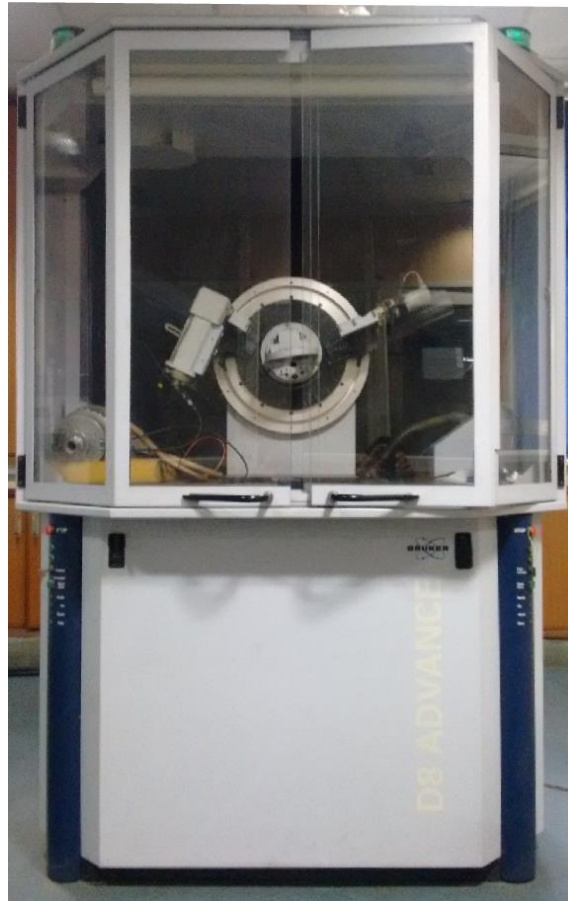


Fig. 4.11: X-Ray diffractometer in DTU, Delhi

4.7 Micro hardness tester

Micro Hardness Tester is a key piece of equipment that is indispensable to metallographic research, product quality control, and the development of product certification materials.

Vickers Micro hardness test procedure as per ASTM E-384, EN ISO 6507, and ASTM E-92 standard specifies making indentation with a range of loads using a diamond indenter which is then measured and converted to a hardness value. For this purpose, as long as test samples are carefully and properly prepared, the Vickers Micro hardness method is considered to be very useful for testing on a wide type of materials, including metals, composites, ceramics, or applications such as testing foils, measuring surface of a part, testing individual microstructures, or measuring the depth of case hardening by sectioning a part and making a series of indentations. Two types of indenters are generally used for the

Vickers test family, a square base pyramid shaped diamond for testing in a Vickers hardness tester and a narrow rhombus shaped indenter for a Knoop hardness tester.

The Vickers hardness test method requires a pyramidal diamond with square base having an angle of 136° between the opposite faces. Upon completion of indentation, the two diagonals will be measured and the average value will be considered.

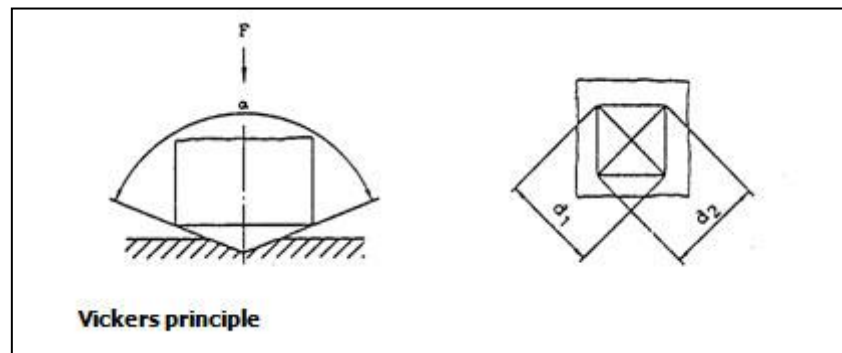


Fig. 4.12: Vickers micro hardness indentation

The loads for Micro Vickers or Knoop hardness testing methods are typically very low, ranging from a few grams to 2 kg. The load range for Macro Vickers hardness test procedure can range up to 50 kgs. Normally the prepared specimens; using metallographic mounting presses are mounted in a plastic medium to facilitate the preparation and testing. In order to enhance the resolution of measurement, the indentations should be as large as possible. The micro hardness was measured with the help of Vickers micro hardness tester. It was compatible with computer; the indentations formed by indenter can be seen. The load can be takes over the micro hardness tester was upto 100 kg. And the magnification of the indentation was 200 x and 400X. The load selected was 5 gm, because at high load the indenter would be large. The magnification chosen was 400 X, because at that low load indentation was very small.

CHAPTER 5

ANALYSIS BY SIMULATION SOFTWARE

ABAQUS (version 6.10) is a finite element program, which is used for the simulations of the engineering real life problem. The software uses three different stages that are pre-processing, solution & post processing to solve problems. There are ten module define in this software. Pre-processing stage involves the creation of geometry and preparation of FEM model, defining Element Type, Material Property & Interaction. In Solution stage, ABAQUS software generates matrices that describe the behavior of each node and element, computes the unknown values of output field variables such as Contact Pressure, Temperature, Heat Distribution etc. In the post processing stage that is Visualization. In this stage results can be analyzed and plotted.

ABAQUS is a software application used for both the modelling and analysis of mechanical components and assemblies (pre-processing) and visualizing the finite element analysis result. It is a general-purpose Finite-Element analyzer that employs implicit integration scheme. This runs as a background process and does the real numerical calculations. After completion of simulation, the results can be monitored in the post processing phase. ABAQUS is also used to view, plot and process the data.

There are 9 modules to perform analysis in ABAQUS.

5.1 Part Module

Two solid models are to be created in this module, which are pin and disc

- **Dimension of pin-** Diameter: 8 mm & Height: 40mm

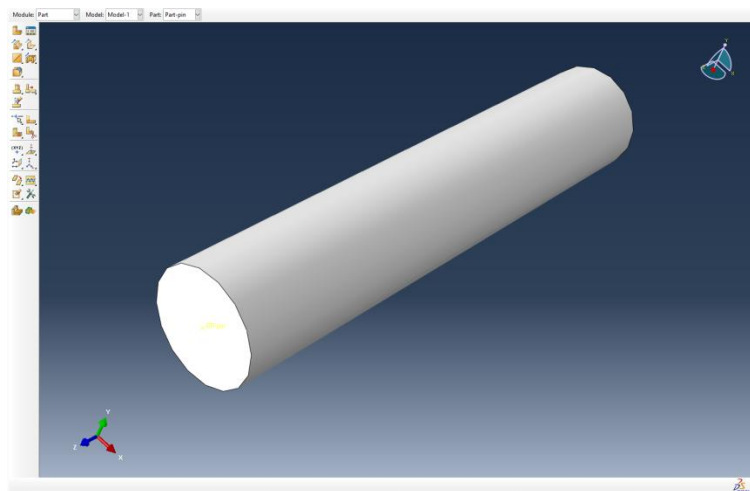


Fig. 5.1: 3D Model of pin

- **Dimension of sample plate-**

Side length of square plate: 100mm & Thickness: 2mm

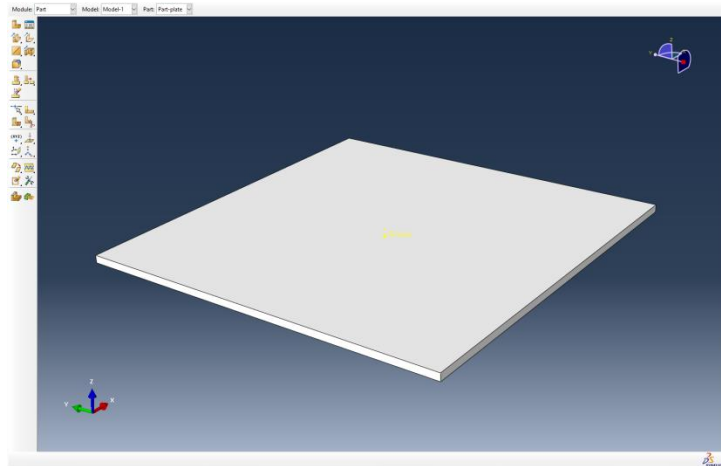


Fig. 5.2: 3D model of sample plate

5.2 Property Module

Two materials are to be defined by their properties and then materials are assigned to the sections and then the sections are assigned to the parts respectively.

- **Coating Material-** It is the mixture of four materials namely NiCr, CrC, Mo and Fe+Mo with specific proportions are to be taken.

Table 5.1 Composition of sample material

Powder name	Composition (grams)
Molybdenum iron alloy (Mo+Fe)	600
Molybdenum (Mo)	200
Nickel Chromium Alloy (NiCr)	100
Chromium Carbide(CrC)	100

- We find out the properties of coating which is shown in table 5.2 for simulation by taken molar average of the properties of main four constructive material Fe+Mo, Mo, CrC and NiCr.

Table 5.2 Properties of materials

Material Properties	Fe+Mo	Molybdenum	Nickel Chromium	Chromium Carbide	Coating Material
Young's Modulus (GPa)	233.4	330	220	373.13	265.353
Poisson's Ratio	0.3086	0.38	0.26	0.22	0.30916
Density (Kg/m³)	8284	10300	8400	6680	8538.4
Thermal Conductivity (W/mK)	52.32	138	11.3	189.77	79.099
Thermal Expansion Coefficient (m/mK)	12.388*10 ⁻⁶	5.5*10 ⁻⁶	14*10 ⁻⁶	4.9*10 ⁻⁶	10.4228*e⁻⁶
Specific Heat (J/KgK)	451.6	250	450	460	411.96

Table 5.3 properties of pin and disc materials

Properties of material	Material properties of pin	Material properties of disc
Young's Modulus	120 GPa	265.353 GPa
Poisson's Ratio	0.26	0.309
Specific Heat	460.54 J/KgK	411.96 J/KgK
Conductivity	46 W/mK	79.1 W/mK
Density	7200 Kg/m ³	8538.4 Kg/m ³
Expansion coefficient	11*10 ⁻⁶ m/mK	10.42 10 ⁻⁶ m/mK

5.3 Assembly Module

Recall the parts in the assembly and define their position with respect to each other parts. 'Part-pin' and 'Part-Disc' are recalled in assembly and define the position of pin from the centre according to the conditions. Then define constraint between the mating surfaces as face to face constraint.

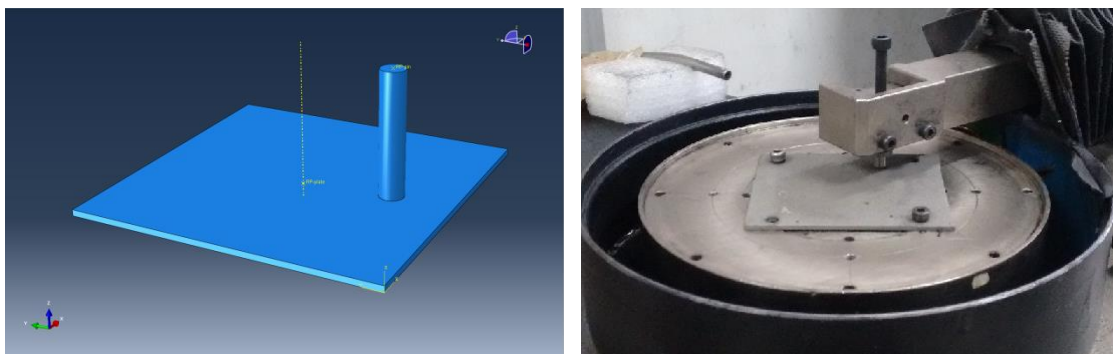


Fig. 5.3: Assembly of pin on disc

5.4 Step Module

First step is initial step which is auto generated to solve the boundary conditions first step without loading. Then according to problem we can select number of steps. In this case we select the coupled-temperature-displacement-analysis.

- Period: 10 seconds
- Max. Number of increments: 1000
- Initial increment size: 0.01
- Minimum increment size: 0.00001
- Maximum increment size: 0.1
- Maximum temperature increment size per increment: 10⁰C.

Field Output- Select the output variables in this manager which are required as results.

- Contact pressure
- Temperature
- Translation and rotational
- Heat flux vector

5.5 Interaction Module

Define the Interaction between the mating parts. In Pin on Disc analysis frictional contact is define between the surfaces and also the properties of interaction is also define like friction coefficient, normal and tangential behaviour. Constraints are also defined in this module.

Interaction Property

- **Normal behavior-** This property is defined for all three types of boundary conditions which is hard contact type.
- **Tangential behavior-** It is defined separately for all three conditions as follows.

Table 5.4 Interaction properties for load 50 N

Interaction	Contact Property	Friction formulation	CoF
Disc surface/ Pin surface	Tangential behavior	Penalty	0.4

Table 5.5 Interaction Properties for load 60N

Interaction	Contact Property	Friction formulation	CoF
Disc surface/ Pin surface	Tangential behavior	Penalty	0.38

Table 5.6 Interaction Properties for load 70N

Interaction	Contact Property	Friction formulation	CoF
Disc surface/ Pin surface	Tangential behavior	Penalty	0.3

- **Heat generation-** Heat is generated between the pin and disc rubbing surfaces due to friction. Generated frictional heat conducted to pin surface (slave surface) as a factor of 0.115 which is depend on the properties of material. This value is same for all three boundary condition as there is no change in material composition.

5.6 Load module

In this module loads and boundary conditions are to be defined for the analysis.

Table 5.7 Boundary conditions for three different loading conditions

Track Diameter	60mm	50mm	40mm
Sliding velocity	1m/s	2m/s	3m/s
Load	50N	60N	70N
Sliding distance	2500m	2500m	2500m
Time	2500s	1250s	834s
RPM	319	764	1433
Angular velocity	33.4 rad/s	80 rad/s	150 rad/s
Pressure	613281 Pa	735937 Pa	858594 Pa

- Pressure will apply on the above face of Pin.
- Angular velocity is defined to the Reference point of the disc which rotates the whole disc about its centre.
- **Boundary condition for pin-** Freeze 3 rotational and 2 translational motion of the pin, only one translational motion of the pin in the z direction or perpendicular to disc is free.
- **Boundary condition for disc-** Freeze 3 translational and 2 rotational motion of the disc, only one rotational motion of the disc is free about z axis or which is along the centre line of the disc.
- Predefined field manager is defined the temperature of part at initial step which is 24°C as atmospheric condition.

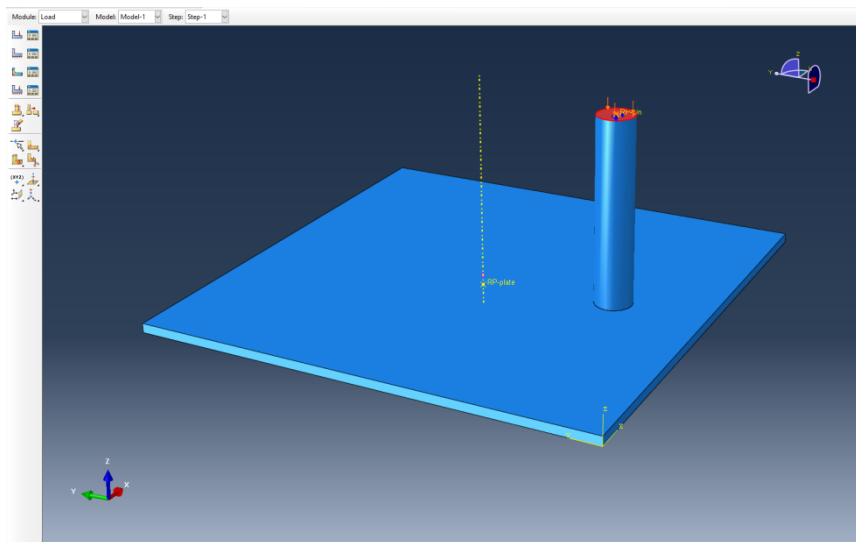


Fig. 5.4: Loading Condition

5.7 Mesh module

Pin and plate is taken as dependent part assembly so the meshing is to done separately for both parts. And the element type for the 50N, 60N and 70N loading condition we choose element type is C3D8T for both pin and plate whose shape is hexagonal. All the elements are from family of coupled temp displacement type.

- **Pin-** **Element shape-** Hexagonal
Element family- Coupled temperature-displacement type
Geometric order- Linear
Number of elements-540
- **Plate-** **Element Shape-** Hexagonal
Element family- Coupled temperature-displacement type
Geometric order- Linear
Number of elements-1089

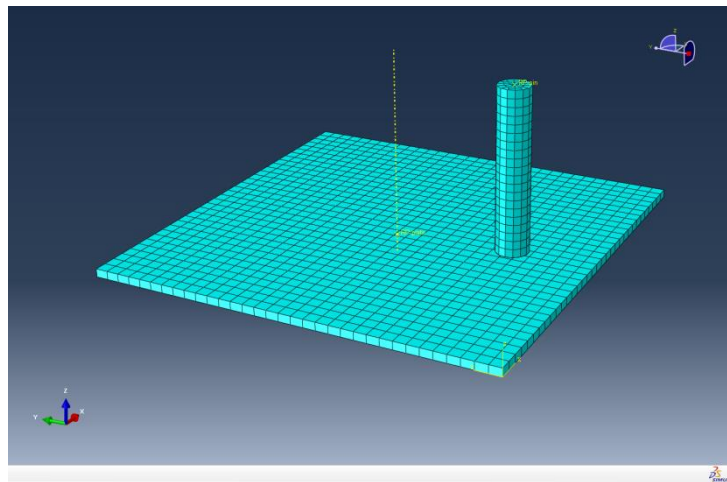


Fig. 5.5: Meshed Assembly View

5.8 Job Module

In this module, analysis of the solution is done by particular solution technique full newton method. Solution of the problem is done in incremental steps.

5.9 Visualization

In this module, the result of output variables is shown by the image, animation and graphs for every node and element. The result of temperature and contact pressure is shown on the animation.

CHAPTER 6

RESULTS AND DISCUSSION

In the visualization module the parameters have to be selected for the results. Looking at the animation of the simulation makes clear that the boundary conditions of the pin are chosen properly. There are no extra stresses generated around the boundary conditions at the top pin. Stresses due to the BC's could be clearly seen. When a plot is made of the nodes at the lower surface of the pin part of the z-direction, no meaningful displacement occurs (order 1.10^{-15} in the contact area). This means that the BC of the disc is chosen in the right way as well.

In the step the pressure is equally distributed, because the model has one color at each increment. A top view the disc shows that there is symmetric spot of stresses in the disc around the pin. That it is completely round is due to round form of the pin. An intersection of the disc shows that the thickness of the disc is chosen properly. Large stresses occur only in the upper part of the disc. It can also be seen that at the inside of the pin (near the disc centre) the stresses are higher than at the outside of the pin. When the disc rotates and the normal force is pushing at the top of pin, the pin tends to stick, together with the movement it causes a little bending of the pin. The front of the pin is pushed into the disc and at the back it lifts up a little according to the front. Because the circular movement of the disc the stresses at the inside of the pin are higher than at the outside of the pin.

For model robustness, the different values of the quantities have to be checked. The values that will be checked are summarized below. An approach of what the values should be, are calculated with the equations presented in chapter 3. The prescribed values should have a certain value at a certain point in the simulation.

1. The contact pressure in the last increment of the first step should be equal to the applied pressure.
2. The magnitude of the reaction forces should be around $F_{CoF} = N \cdot \mu$
3. The rotational displacement of the nodes should be equal to what is prescribed, $\omega = 2\pi N/60$ [rad/s].

Table 6.1: Angular velocities of disc

N (rpm)	ω (rad/s)
319	33.4
764	80
1433	150

1. Contact pressure

The values of contact pressure are obtained in visualization model under CPRESS drop down menu. The value of contact pressure is recorded for every step to get the wear depth. It can be seen that the magnitude of contact pressure is increasing by increasing the load at the constant speed.

Fig.: 6.1 presents the contact pressure distribution at the disc surface, showing a non-uniform stress field under the flat pin surface contact. Higher pressure values are observed along the edge of the contact of the pin with the disc, which can lead to local wear and plastic deformation effects. In fact, pressure contact on disc is also evaluated for the wear calculation of material AISI H13 of disc [21]. This singularity in contact pressure field is verified also in the contact of a flat punch with a plane [22].

- **At 70 N load and RPM 1433** – Maximum value of contact pressure is 858593.75 Pa which is at the interface of the contact. Value of contact pressure is uniform through the pin and disc contact area. Meshed elements are of hexagonal so they uniformly distributed.

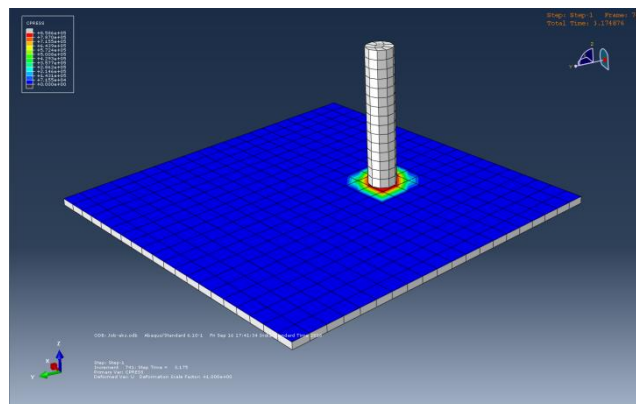


Fig.6.1: Contact Pressure at 70N loading condition

- **At 60N load and RPM 764-** Maximum value of contact pressure is 735937.5 Pa which is at the interface of the contact. Meshing is tetrahedron so the representation of contact pressure is not circular.

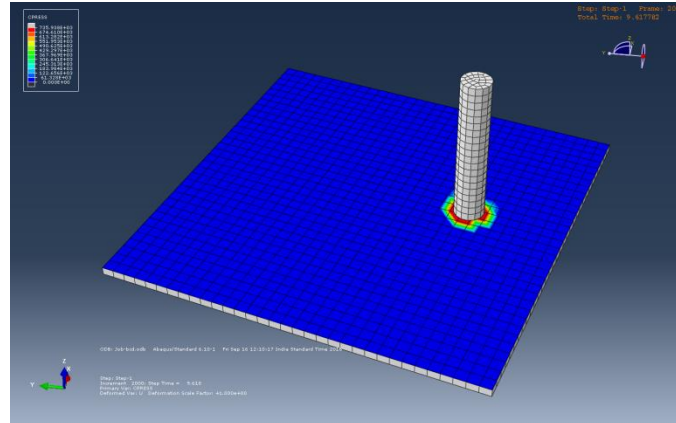


Fig. 6.2: Contact Pressure at 60N loading condition

- **At 50N load and RPM 319-** Maximum value of contact pressure is 613281 Pa which is at the interface of the contact. as the above condition. Here is also the mesh shape is tetrahedron so the representation of contact pressure is not circular.

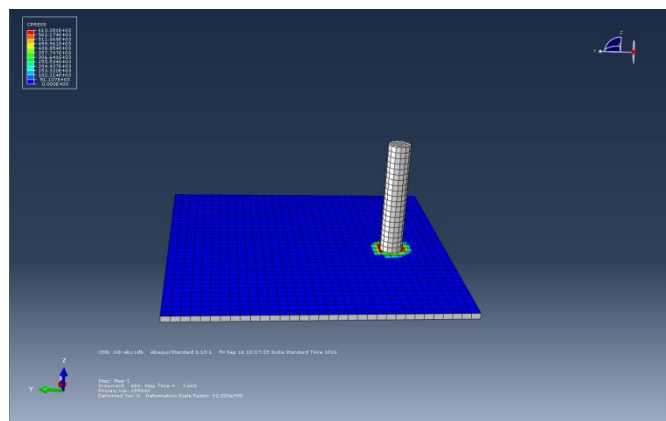


Fig. 6.3: Contact Pressure at 50N loading condition

The values of the contact pressure are shown at 50N, 60N and 70N loading conditions for the time period of 10 seconds.

Table 6.2 Contact pressures according to load

Loading conditions	70N load	60N load	50N load
Contact pressure (Pa)	858594	735937	613281

Graphical representation of contact pressure at interface of pin and disc shows the straight lines which are horizontal in nature tells that the contact pressure is constant throughout the simulation.

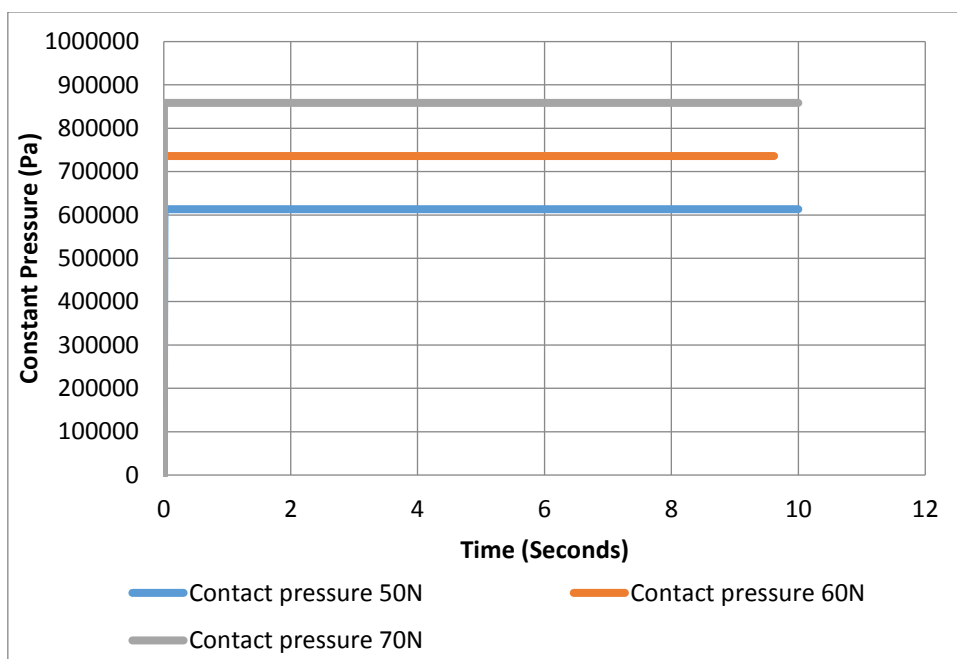


Fig. 6.4: Contact pressures at the contact interface of pin and disc

2. Temperature distribution

- **Load at 70N and RPM 1433-** Maximum value of for the temperature for this loading condition is about 45°C after 10 seconds of period which is at contact point of pin and disc. As the disc rotate a particular point on the disc firstly in a contact then it remains without contact for a short of time then again it comes into contact and goes off. Cycle continued as a result, temperature of disc increases but with up down graph.

Right side image is shows the variation of temperature of pin on disc setup and the maximum temperature is 48°C while performing experiment after 10 seconds. This thermal image is taken by pyrometer.

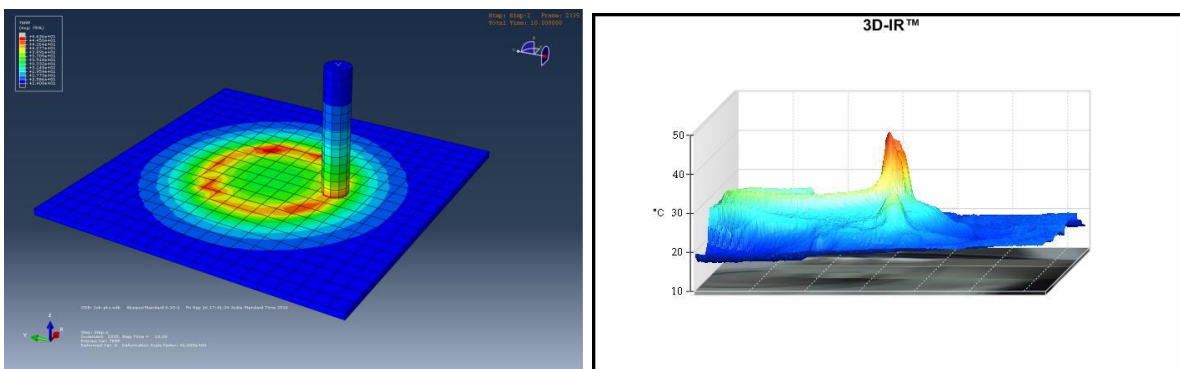


Fig. 6.5: Temperature by ABAQUS and experiment at 70N loading

- **Load at 60N and RPM 764-** Maximum value of for the temperature for this loading condition is about 38°C after 10 seconds of period which is at contact point of pin and disc. Temperature of disc increases with variations because of rotational motion of disc. Right side image is shows the variation of temperature of pin on disc setup and the maximum temperature is 40°C while performing experiment after 10 seconds. This thermal image is taken by pyrometer.

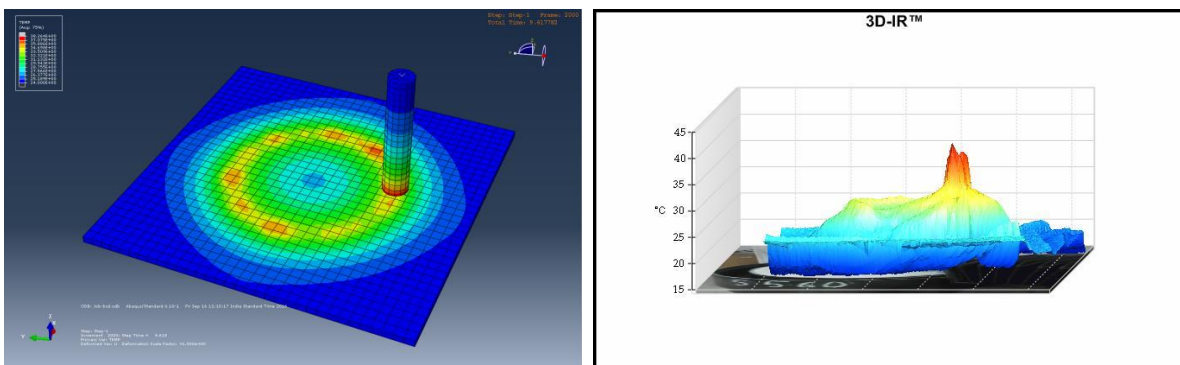


Fig.6.6: Temperature by ABAQUS and experiment at 60N loading

- **Load at 50N and RPM 319-** Maximum value of for the temperature for this loading condition is about 32⁰C after 10 seconds of period which is at contact point of pin and disc. Temperature of disc increases with variations because of rotational motion of disc.

Right side image is shows the variation of temperature of pin on disc setup and the maximum temperature is 33⁰C while performing experiment after 10 seconds. This thermal image is taken by pyrometer.

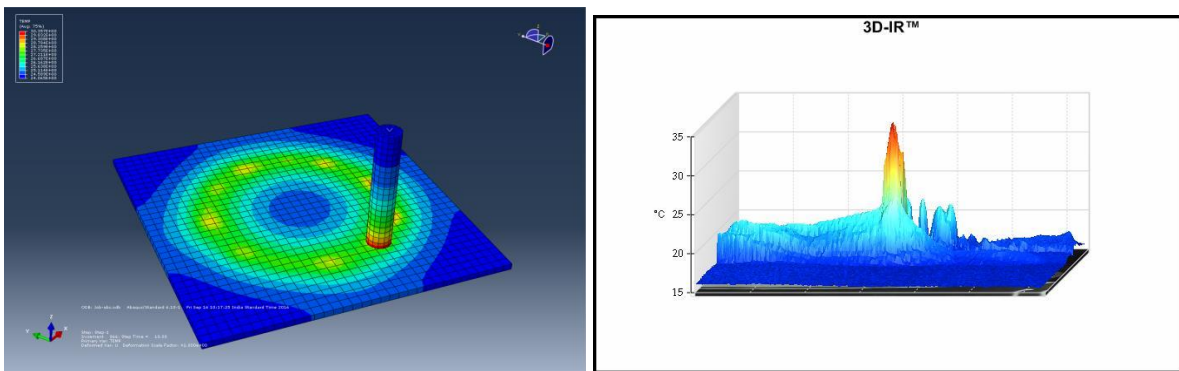


Fig.6.7: Temperature by ABAQUS and experiment at 50N loading

The values of the temperature are shown at 50N, 60N and 70N loading conditions after the time period of 10 seconds.

Table 6.3 Contact pressures according to load

Loading conditions	70N load	60N load	50N load
Temperature (°C) by ABAQUS	44	39	32
Temperature (°C) by experiment	48	40	33

Graphical representation of temperature at interface of pin on disc during the time period of 10 seconds

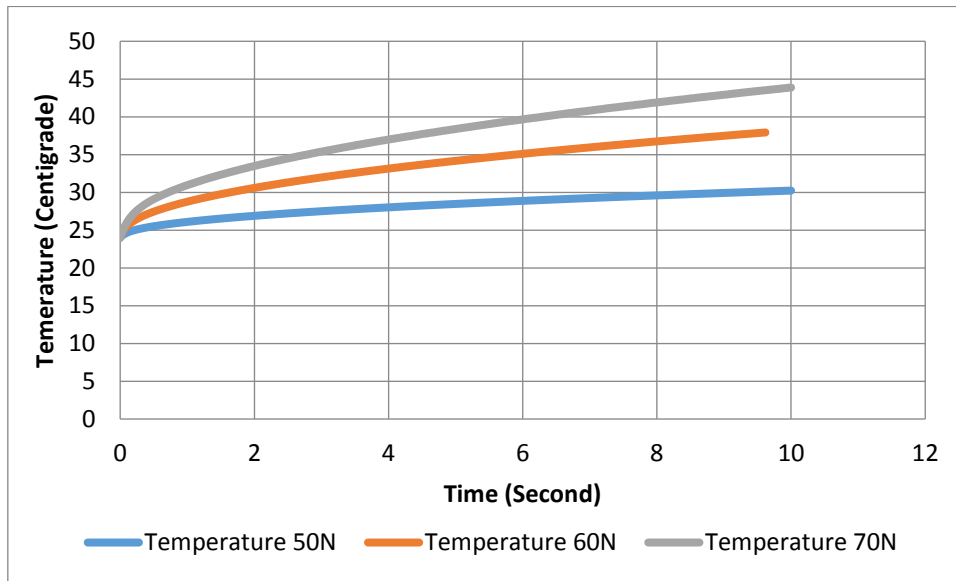


Fig.6.8: Temperature at the contact interface of pin and disc

3. Heat flux Vector distribution

This parameter shows the heat flow per unit area which is generated due to friction between the contact surfaces. One part of energy goes to the frictional losses between pin and disc contact because of this heat is generated between at the interface. Generated heat is conducted to the pin and disc with specific factor. This factor value is 0.151 for the slave surface (bottom surface of pin) it depends on the physical properties of both the materials.

- **At Load 70N and RPM 1433-** Maximum value of HFL is 87.375 kJ/m^2 at the sliding contact.

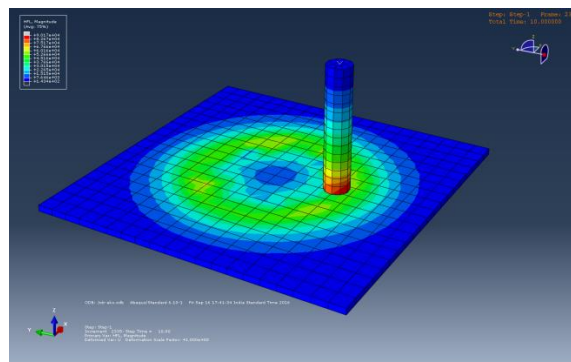


Fig. 6.9: Heat flux vector distribution at 70N loading condition

- **At load 60N and RPM 764-** Maximum value of HFL is 61.154 kJ/m² at the sliding contact.

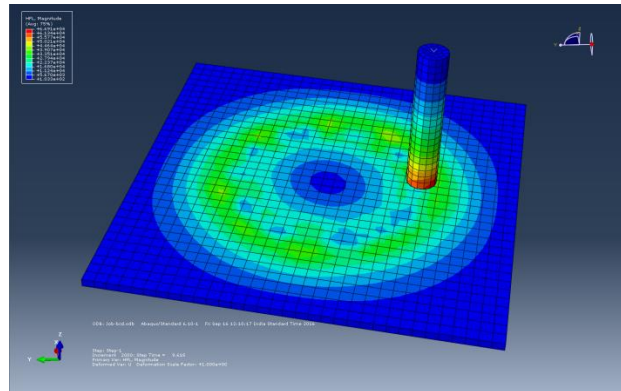


Fig. 6.10: Heat flux vector distribution at 60N loading condition

- **At load 50N and RPM 319-** Maximum value of HFL is 26.879 kJ/m² at the sliding contact.

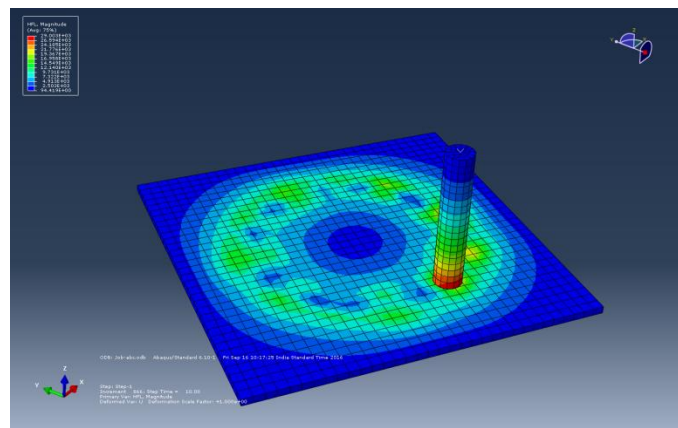


Fig. 6.11: Heat flux vector distribution at 50N loading condition

From the above results it is clear that the heat flux increases with increase in the value of load and the value of rotational speed. So the heat distribution pattern in 70N loading condition is more and high concentration as compared to the 60N and 50N loading conditions.

The following graph provides you a clearer picture to understand the heat distribution on the plate. At the starting time heat distribution's time gradient value is high because of low temperature but as the time increases heat distribution's time gradient value decreases and becomes constant and appears that the gradient is zero.

Graphical representation of Heat Flux Vector at interface of pin on disc during the time period of 10 seconds

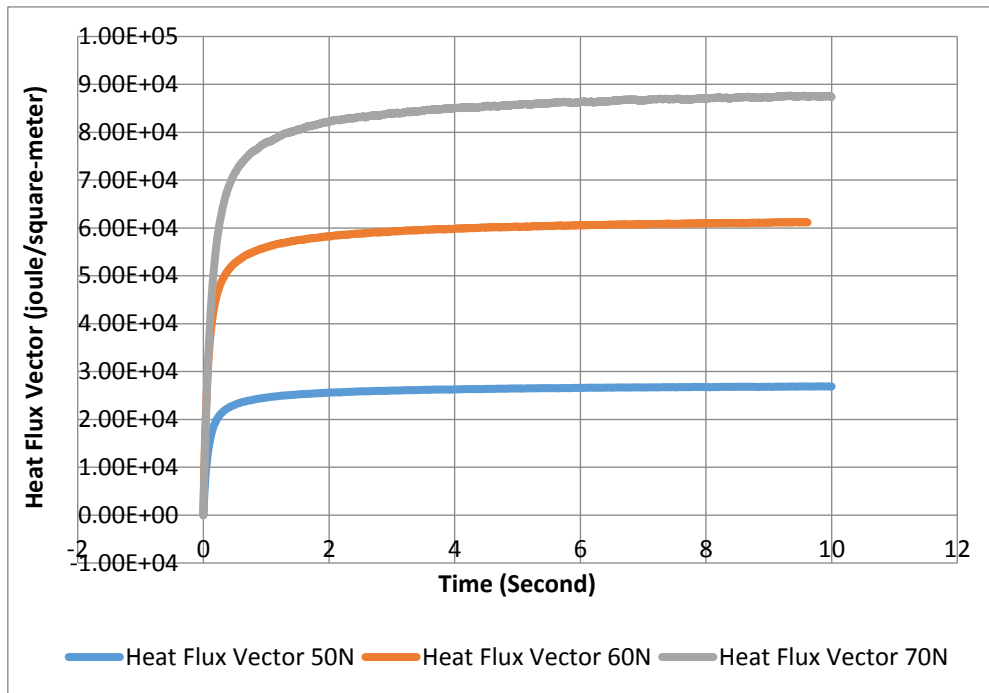


Fig.6.12: Heat Flux Vector at the contact interface of pin and disc

4. Coefficient of friction

In terms of friction coefficient, experimental tests were conducted for shorter time periods when loads were different 50 N, 60N and 70 N and rotational speed 319 RPM, 764 RPM and 1433 RPM respectively for high wear on the disc surface. In these tests, friction coefficient curves show with the sliding distance, as seen in Fig. 6.12. Average value of frictional coefficient for the load 70N, 60N and 50N are 0.42, 0.409 and 0.368 respectively. Similarly, average values of frictional coefficient for AlCrN and AlCrN-T are 0.7 and 0.3 respectively for 300 meter of running distance [23] average value of frictional coefficient is 0.8 for the pin of material AISI 4140 and disc of material H13 [21] for high wear rate test of pin.

In ABAQUS Software we take the average value of coefficient of friction for respective load. For 50N, 60N & 70N loads the value of CoF are 0.4, 0.38 & 0.3 respectively. The value of CoF in simulation does not change with time and remains constant.

The following graph shows the variation in CoF for experimental analysis with respect to their sliding distance travelled.

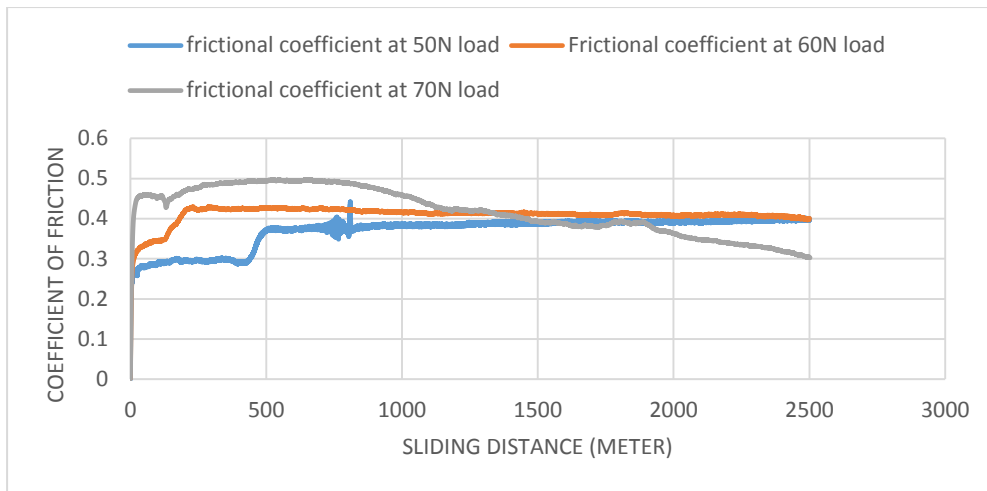


Fig. 6.13: Frictional coefficient of coating material between pin and disc

5. Specific wear rate

The value for Specific wear rate rate is differing according to the loading conditions. As the load and the rotational velocity increases specific wear rate also increases with nonlinearly as shown in the fig: 6.13.

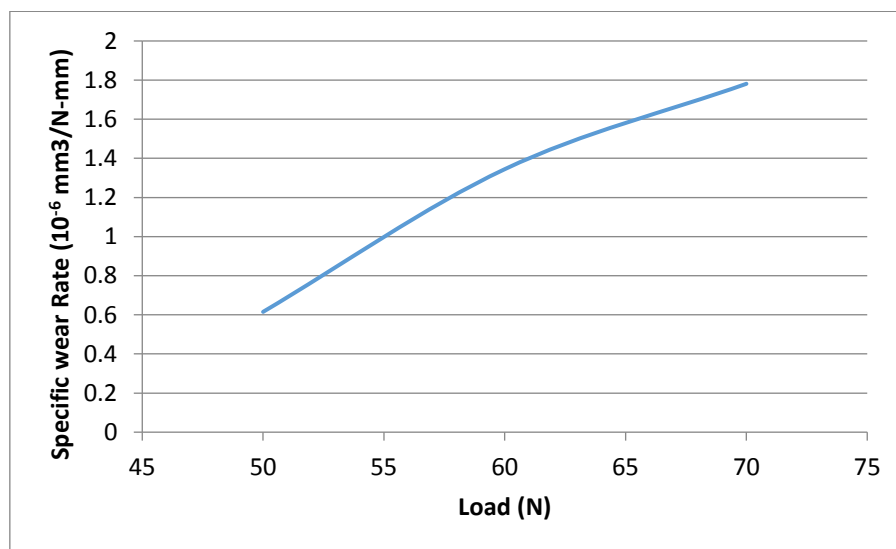


Fig. 6.14: Specific wear rate vs load

It can be seen from Table 3.5 that the wear volume of coating material varies from 76.89 to 311.675, while the wear coefficient K varies from 6.1512×10^{-7} to 1.781×10^{-6} , depending on the disc material used. It is noted that the wear rates have their highest values with maximum load and rotation condition their lowest values with lowest load and rotation condition. The

wear rates also vary a lot from the type of disc material and the testing method used, about "61% and "55% from the mean value obtained from the moving pin and stationary pin tests, respectively. On the other hand, the wear coefficient values obtained do not vary significantly with the disc materials used. The variation is about "4% and "17% from the mean value obtained from the moving pin and stationary pin tests respectively [32].

Table 3.5 specific wear rate and coefficient of friction with respect to load

Load	50N	60N	70N
Specific wear rate (mm³/N-mm)	6.1512 * 10 ⁻⁷	1.34453 * 10 ⁻⁶	1.781* 10 ⁻⁶
Wear volume (µm³)	76.89	201.6795	311.675
Coefficient of friction	0.368	0.409	0.42

CHAPTER 7

CONCLUSION AND FUTURE SCOPE

7.1 Conclusion

According to results and simulations conducted in this work allowed the following conclusions:

- The specific wear rate and the average value of friction coefficient is increases as load increases.
- Temperature profile at the frictional contact interface by simulation is approximately similar to the profile of temperature get by the experimental results by variation of temperature are found in experiment by the debris created by abrasion mechanism.
- Wear volume also increases as load increases but after a long run period of wear, wear rate decrease significantly because of resistive oxide layer of molybdenum formed which decreases the wear rate significantly.

7.2 Future scope

Tribology is the vast field of science, simulation of tribological problem gives a numerical analysis of the triobological problems and real life. The main future perspectives of this research work are as follows:

- Different combination of pin and disc material can be explored and simulated with giving different roughness to the mating surfaces.
- A more advance software technology can be used in future to analyze the simulation more accurately.
- Frictional contact model problems are to be solved by making a solver using programming in FORTRAN.

REFERENCES

1. Theo Mang, Kirsten Bobzin and Thorsten Bartels “Industrial Tribology: Tribosystems, Friction, Wear and Surface” volume 1 page no 197.
2. GOETZE Piston Ring Handbook
3. Gwidon W. Stashowiak, Andrew W. Batchelor and Grazyna B. Stachowiak, text book of “Experimental Methods in Tribology”.
4. Bortoleto, E. M., Rovani, A. C., Seriacopi, V., Profito, F. J., Zachariadis, D. C., Machado, I. F., & Souza, R. M. D. (2013). Experimental and numerical analysis of dry contact in the pin on disc test. *Wear*, 301(1), 19-26.
5. Kennedy, F. E., Lu, Y., & Baker, I. (2015). Contact temperatures and their influence on wear during pin-on-disk tribotesting. *Tribology International*, 82, 534-542.
6. Li, X., Sosa, M., & Olofsson, U. (2015). A pin-on-disc study of the tribology characteristics of sintered versus standard steel gear materials. *Wear*, 340, 31-40.
7. Verma, P. C., Menapace, L., Bonfanti, A., Ciudin, R., Gialanella, S., & Straffelini, G. (2015). Braking pad-disc system: Wear mechanisms and formation of wear fragments. *Wear*, 322, 251-258.
8. Zmitrowicz, A. (2006). Wear patterns and laws of wear—a review. *Journal of theoretical and applied mechanics*, 44(2), 219-253.
9. S.Guicciardi, C. Melandri, F. Lucchini, G. De Portu, “On data dispersion in pin-on-disk wear tests”, *Wear* 252 (2002) 1001–1006.
10. Priit Poõdra, Soõren Andersson, “Simulating sliding wear with finite element method”, *Tribology International* 32 (1999) 71–81.
11. P.Prabhu et al, “Experimental Study and Verification of Wear for Glass Reinforced Polymer using ANSYS.
12. ImamSyafa at al, “Prediction of Sliding Wear of Artificial Rough Surfaces”.
13. Lim, S. C., Ashby, M. F. and Brunton, J. H., Wear-rate transitions and their relationship to wear mechanisms. *Acta Metall.*,1987, 35, 1343–1348.
14. Yang, L. J. (2004). Wear coefficient of tungsten carbide against hot-work tool steel disc with two different pin settings. *Wear*, 257(5), 481-495.
15. Wang, Y., Brogan, K., & Tung, S. C. (2001). Wear and scuffing characteristics of composite polymer and nickel/ceramic composite coated piston skirts against aluminum and cast iron cylinder bores. *Wear*, 250(1), 706-717.

16. Novak, R., & Polcar, T. (2014). Tribological analysis of thin films by pin-on-disc: evaluation of friction and wear measurement uncertainty. *Tribology International*, 74, 154-163.
17. Tului, M., Ruffini, F., Arezzo, F., Lasisz, S., Znamirovski, Z., & Pawlowski, L. (2002). Some properties of atmospheric air and inert gas high-pressure plasma sprayed ZrB₂ coatings. *Surface and Coatings Technology*, 151, 483-489
18. He, P. F., Ma, G. Z., Wang, H. D., Yong, Q. S., Chen, S. Y., & Xu, B. S. (2016). Tribological behaviors of internal plasma sprayed TiO₂-based ceramic coating on engine cylinder under lubricated conditions. *Tribology International*.
19. Johansson, S., Nilsson, P. H., Ohlsson, R., & Rosén, B. G. (2011). Experimental friction evaluation of cylinder liner/piston ring contact. *Wear*, 271(3), 625-633.
20. Wang, Y., Jiang, S., Wang, M., Wang, S., Xiao, T. D., & Strutt, P. R. (2000). Abrasive wear characteristics of plasma sprayed nanostructured alumina/titania coatings. *Wear*, 237(2), 176-185.
21. Sivkov, A., Shanenkov, I., Pak, A., Gerasimov, D., & Shanenkova, Y. (2016). Deposition of a TiC/Ti coating with a strong substrate adhesion using a high-speed plasma jet. *Surface and Coatings Technology*, 291, 1-6.
22. Peat, T., Galloway, A. M., Toumpis, A. I., & Harvey, D. (2016). Evaluation of the synergistic erosion-corrosion behaviour of HVOF thermal spray coatings. *Surface and Coatings Technology*, 299, 37-48.
23. Fu, G., Wei, L., Shan, X., Zhang, X., Ding, J., Lv, C., & Ye, S. (2016). Influence of a Cr₂O₃ glass coating on enhancing the oxidation resistance of 20MnSiNb structural steel. *Surface and Coatings Technology*, 294, 8-14.
24. Verdon, C., Karimi, A., & Martin, J. L. (1997). Microstructural and analytical study of thermally sprayed WC-Co coatings in connection with their wear resistance. *Materials Science and Engineering: A*, 234, 731-734.
25. Shi, X., Wang, C., Lin, H., Huo, C., Jin, X., Shi, G., & Dong, K. (2016). Oxidation resistance of a La–Mo–Si–O–C coating prepared by Supersonic Atmosphere Plasma Spraying on the surface of SiC-coated C/C composites. *Surface and Coatings Technology*, 300, 10-18.
26. Bartuli, C., Valente, T., & Tului, M. (2002). Plasma spray deposition and high temperature characterization of ZrB₂–SiC protective coatings. *Surface and Coatings Technology*, 155(2), 260-273.

27. Withey, E., Kruiuzenga, A., Andraka, C., & Gibbs, P. (2016). Plasma sprayed coatings for containment of Cu-Mg-Si metallic phase change material. *Surface and Coatings Technology*, 304, 117-124.
28. Zhang, Y., Hu, H., Zhang, P., Hu, Z., Li, H., & Zhang, L. (2016). SiC/ZrB 2–SiC–ZrC multilayer coating for carbon/carbon composites against ablation. *Surface and Coatings Technology*, 300, 1-9.
29. Bergan, P. G., Horrigmoe, G., Bråkeland, B., & Søreide, T. H. (1978). Solution techniques for non– linear finite element problems. *International Journal for Numerical Methods in Engineering*, 12(11), 1677-1696.
30. Hibbitt, H. D., and B. I. Karlsson, “Analysis of Pipe Whip,” EPRI, Report NP–1208, 1979.
31. Abaqus Analysis User's Guide.